SERBP1 interacts with PARP1 and is present in PARylation-dependent protein complexes regulating splicing, cell division, and ribosome biogenesis

Kira Breunig[1,†], Xiufen Lei[1,†], Mauro Montalbano[2,3†], Gabriela D. A. Guardia[4], Shiva Ostadrahimi[1,5], Victoria Alers[1,5,6], Adam Kosti[1,5], Jennifer Chiou[7], Nicole Klein[1], Corina Vinarov[1], Lily Wang[1], Mujia Li[1], Weidan Song[8], W. Lee Kraus[8], David S. Libich[1,6], Stefano Tiziani[7,9,10], Susan T. Weintraub[6], Pedro A. F. Galante[4] and Luiz O. F. Penalva[1,5,*]

[1] Children's Cancer Research Institute, UT Health San Antonio, San Antonio, Texas, 78229, USA
[2] Mitchell Center for Neurodegenerative Diseases, University of Texas Medical Branch, Galveston, TX, USA
[3] Department of Neurology, University of Texas Medical Branch, Galveston, TX, USA
[4] Centro de Oncologia Molecular, Hospital Sírio-Libanês, São Paulo, São Paulo, 01309-060, Brazil
[5] Department of Cell Systems and Anatomy, UT Health San Antonio, San Antonio, Texas, 78229, USA
[6] Department of Biochemistry and Structural Biology, UT Health San Antonio, San Antonio, Texas, 78229, USA
[7] Department of Nutritional Sciences, College of Natural Sciences, University of Texas at Austin, Austin, TX, USA
[8] Laboratory of Signaling and Gene Regulation, Cecil H. and Ida Green Center for Reproductive Biology Sciences, The University of Texas Southwestern Medical Center, Dallas, TX, USA
[9] Department of Pediatrics, Dell Medical School, University of Texas at Austin, Austin, TX, USA
[10] Department of Oncology, Dell Medical School, University of Texas at Austin, Austin, TX, USA

[†] Joint Authors
* To whom correspondence should be addressed. Tel: +12105629049; Fax: +12105629016; Email: penalva@uthscsa.edu

Keywords: SERBP1, RNA binding protein, PARP1, G-quadruplex, interactome, proteomics, mass spectrometry

Running title: SERBP1 novel regulatory roles in conjunction with PARP1 and PAR-binders

ABSTRACT

RNA binding proteins (RBPs) containing intrinsically disordered regions (IDRs) are present in diverse molecular complexes where they function as dynamic regulators. Their characteristics promote liquid-liquid phase separation (LLPS) and the formation of membraneless organelles such as stress granules and nucleoli. IDR-RBPs are particularly relevant in the nervous system and their dysfunction is associated with neurodegenerative diseases and brain tumor development. Serpine1 mRNA-binding protein 1 (SERBP1) is a unique member of this group, being mostly disordered and lacking canonical RNA-binding domains. We defined SERBP1's interactome, uncovered novel roles in splicing, cell division and ribosomal biogenesis, and showed its participation in pathological stress granules and Tau aggregates in Alzheimer's brains. SERBP1 preferentially interacts with other G-quadruplex (G4) binders, implicated in different stages of gene expression, suggesting that G4 binding is a critical component of SERBP1 function in different settings. Similarly, we identified important associations between SERBP1 and PARP1/polyADP-ribosylation (PARylation). SERBP1 interacts with PARP1 and its associated factors and influences PARylation. Moreover, protein complexes in which SERBP1 participates contain mostly PARylated proteins and PAR binders. Based on these results, we propose a feedback regulatory model in which SERBP1 influences PARP1 function and PARylation, while PARylation modulates SERBP1 functions and participation in regulatory complexes.

INTRODUCTION

RNA binding proteins (RBPs) are a diverse group of regulators with 1,500 members cataloged in the human genome (1, 2). They display a variety of RNA binding domains (RRMs, zinc-fingers, KH domains, dsRBD, etc.) and control multiple stages of gene expression, including RNA processing (splicing, capping, 3' end processing, and polyadenylation), modification, transport, decay, localization, and translation (2, 3). RBPs are particularly relevant in the nervous system, where they regulate critical aspects of neurogenesis, neuronal function, and nervous system development (4, 5). Alterations in RBP expression and function are linked to neurological disorders, neurodegenerative diseases, and brain tumor development (6–12).

RBPs assemble in complexes to regulate gene expression. RBP interactions can take place in the context of macromolecular complexes associated with liquid-liquid phase separation (LLPS). This process supports important regulatory environments and is the foundation for membraneless organelles such as stress granules, Cajal bodies, nucleoli, and P-bodies (13–15). RBPs in LLPS tend to share characteristics that include intrinsically disordered regions (IDRs) and RGG boxes. IDR-RBPs can interact with RNA without the presence of specific folded RNA-binding domains (16). These features provide unique structural and biophysical characteristics to dynamically regulate translation, stress response, RNA processing, and neuronal function (17).

Many RBPs in LLPS share a binding preference for G-quadruplexes (G4s). G4s are complex DNA or RNA structures that display stacked tetrads of guanosines stabilized by Hoogsteen base pairing. They function as regulatory elements in different stages of gene expression, promote LLPS, and are implicated in cancer, viral replication, neurodegenerative diseases, neurological disorders, and prion diseases (18–21).

RBPs containing IDRs and RGG motifs are particularly relevant in the nervous system. Their misfolding contributes to the formation of pathological protein aggregates in Alzheimer's disease (AD), Frontotemporal Lobar Degeneration (FTLD), Amyotrophic Lateral Sclerosis (ALS), and Parkinson's disease (PD) while their aberrant expression has been linked to glioblastoma development (22–24). SERBP1 (Serpine1 mRNA-binding protein 1) is a unique member of this group of RBPs for being mostly disordered and lacking typical RNA binding domains other than two short RG/RGG motifs (25). SERBP1 is a highly conserved protein with homologs identified in yeast, plants, invertebrates, and vertebrates. SERBP1 is highly expressed in neuronal and glioma stem cells and a decrease in its levels is required for neuronal differentiation (26). In glioblastoma, SERBP1 functions as a central regulator of metabolic pathways, coordinating the expression of related enzymes and associated factors implicated in serine biosynthesis, one-carbon, and 5'-methylthioadenosine (MTA) cycles. Ultimately, SERBP1 impacts methionine production and, consequently histone methylation and the expression of genes implicated in neuronal differentiation (26).

In the present study, we investigated the SERBP1 interactome. Overall, our results established SERBP1 as a multi-regulatory protein, corroborating that RBPs containing IDRs are dynamic and can assemble different complexes. Despite its predominant cytoplasmic localization, SERBP1 is associated with proteins in specific nuclear complexes implicated in splicing regulation, cell division, and ribosome biogenesis. Approximately a third of SERBP1-associated proteins bind to G4s. These proteins are implicated in various stages of gene expression, indicating that G4s function as SERBP1 regulatory motifs in different scenarios. Finally, our study has identified important associations between SERBP1 and PARP1 that suggest a regulatory loop, in which SERBP1 influences PARylation, and PARP activity. At the same time, PARylation of SERBP1 and its partner proteins modulate their association and function.

RESULTS

SERBP1 interactome reveals its associations with diverse regulatory complexes.

To identify SERBP1-associated proteins and molecular complexes in which it is involved, we conducted pull down experiments in 293T cells followed by proteomics analysis. Cells were transfected with pSBP-SERBP1 or pUltra-SERBP1(control). The SBP tag is a short peptide with high affinity for streptavidin. Protein complexes are then isolated via pulldown using streptavidin beads. Analysis by mass spectrometry yielded a high-confidence list of 570 SERBP1-associated proteins. Peptides for these proteins were only present in the pSBP-SERBP1 pull-down samples or displayed a minimum of 3-fold enrichment in comparison to control – **Table S1, Figure S1**. Gene Ontology (GO) analyses (27–29) of identified partners indicated that SERBP1 participates in diverse regulatory complexes in the cytoplasm and nucleus – **Figure 1A-B** and **Table S1**. We compared our data to the results of two large-scale studies that used proximity-dependent biotinylation (Bio ID) (30, 31) to identify protein-protein interactions and checked the datasets in BioGRID (32). 146 SERBP1 interactors identified in our analysis were also identified in other high-throughput studies – **Table S1**.

Although SERBP1's partners indicate its participation in different stages of translation as well as in its regulation, the many associations with translation initiation factors suggest that SERBP1's primary function is in initiation – **Table S1**. As expected, based on previous studies (33–36), we identified several ribosomal proteins associated with SERBP1 – **Table S1**. SERBP1 knockdown in U251 and U343 cells resulted in a decrease of overall translation as shown by puromycin incorporation assays – **Figure S2A**.

SERBP1 is mostly localized in the cytoplasm. SERBP1 nuclear localization increases in response to stress and is regulated by arginine methyltransferases (37–39). SERBP1-associated proteins suggest it participates in nuclear functions; out of 570 associated proteins, 344 display cytoplasmic/nuclear localization, while 100 are exclusively found in the nucleus – **Table S1**. GO analyses of this group identified specific nuclear complexes. The functions of SERBP1-associated proteins suggest that SERBP1 is involved in different stages of ribosome biogenesis – **Table S1**. SERBP1 participation in ribosome biogenesis is corroborated by its presence in nucleoli – **Figure S2B-C**. Results of our previous RIP-Seq analysis (26) and a CLIP-seq study (36) showed that SERBP1 binds preferentially to multiple snoRNAs (**Table S2**) and at specific sites in 18S and 28S rRNA. These results, aligned with the fact that SERBP1 associates with FBL and DKC1, two critical snoRNP components, strongly indicate SERBP1 involvement in rRNA modification. Besides ribosome biogenesis, SERBP1 is also likely involved in different stages of RNA processing, in particular splicing, and telomere maintenance – **Figure 1A-B**.

SERBP1 is a highly conserved protein. In *S. cerevisiae*, SERBP1 homolog is STM1 (40). According to BioGRID (32), 183 proteins were identified as STM1 interactors. Of the 144 identified human homologs, we found that 53 were SERBP1 interactors – **Table S3**. GO analyses of STM1 interactors indicated that STM1 is also a multi-functional protein. Comparisons of enriched GO terms from the SERBP1 and STM1 analyses suggest that several regulatory functions assigned to SERBP1 based on its associated proteins are evolutionarily conserved, including translation, ribosome biogenesis, RNA processing and telomere maintenance – **Table S3**. SERBP1 also has homologs in plants. A recent study in *A. thaliana* established that AtRGG proteins (SERBP1 homologs) interact with ribosomal proteins and proteins involved in RNA processing and transport (41).

SERBP1 preferentially associates with helicases and G-quadruplex binders.

In order to define the characteristics of SERBP1-associated proteins, we cataloged them according to their protein domains using the Pfam database (42) and performed an enrichment analysis. RNA binding and helicase are the two domain families that appeared most often – **Figure 1C, Figure S3,** and **Table S4**. Based on the results of the proteomics analyses and gene expression correlation studies, DDX21, DHX9, and DHX15 are SERBP1's top-associated helicases – **Table S5**.

SERBP1 displays large intrinsically disordered regions (IDRs) (25). IDRs are ubiquitous within biomolecular condensates in the cytoplasm and nucleus created via liquid-liquid phase separation (LLPS). They lead to the formation of membraneless organelles such as stress granules, P-bodies, and nucleoli (43, 44). Roughly 80% of SERBP1-associated proteins contain IDRs (45) and are present in different membraneless organelles, as discussed below – **Figure 1D** and **Table S4**.

SERBP1 is a G-quadruplex (G4) binder (26, 46), as are 38% of its associated proteins (46, 47) – **Table S6**. RBPs, including SERBP1, often use RGG boxes to bind G4 motifs (48, 49). We found that among 93 SERBP1-associated proteins containing RGG boxes (50), 44 are G4 binders – **Figure 1E** and **Table S6**. G4 binders associated with SERBP1 are mostly proteins implicated in translation, mRNA stability, and splicing, indicating that SERBP1 regulation via G4 binding takes place in different scenarios. Among G4 binders, we identified several RNA helicases (e. g. DDX5, DDX21, DDX3X, and DHX9) that enhance translation by unfolding G4s in 5' UTRs (51–54) – **Figure S3, Tables S1** and **S6**. Since SERBP1 lacks helicase domains, interaction with these proteins could be critical for SERBP1 function in translation.

G4s regulate different aspects of the life cycles of RNA viruses (55, 56). GO terms related to viral translation are among those with the highest fold enrichment in our analyses – **Table S1**. In a study to define the SARS-CoV-2 RNA interactome, 168 human proteins were identified (after exclusion of ribosomal proteins and EI3F factors) (57), including SERBP1 and 92 of its associated proteins – **Table S6**. Of those 92 proteins, 52 are G4 binders – **Table S6**.

SERBP1 affects cell division.

SERBP1 has been previously implicated in chromosome segregation and shown to localize in M bodies during mitosis (36). In agreement, GO analyses of SERBP1-associated proteins revealed chromosome segregation as well as several related functions as enriched terms. Examination of proteins linked to these terms indicated that SERBP1 interacts with proteins in chromosomes as well as centrosomes and mitotic spindles – **Figure 2A** and **Table S1**. To evaluate SERBP1's impact on cell division, U251 and U343 SERBP1 knockdown and control cells were exposed to 20 nM of paclitaxel for 24 hours and later stained with α-tubulin and DAPI. In both cases, SERBP1 knockdown cells had markedly increased numbers of polynucleated cells, reflecting mitotic catastrophe – **Figure 2B-D.** SERBP1 involvement in cell division appears to be conserved. STM1, the SERBP1 yeast homolog, is a suppressor of mutations in genes regulating mitosis (58). Confirming that report, our GO analyses of STM1 genetic interactors showed enrichment for cell division – **Table S3**.

We conducted a viability screening with 269 compounds in GBM U343 and U343 over-expressing (OE) SERBP1 (26). Corroborating SERBP1 involvement in cell division, we determined that SERBP1 OE cells are less sensitive to drugs affecting cell division, cell cycle, and DNA replication. Interestingly, three of these drugs (Mitoxantrone, Flavopiridol, and Doxorubicin) are also known to affect rRNA transcription and processing – **Figure 2E-F** and **Table S7**.

SERBP1 interacts with splicing factors and influences splice site selection.

Among identified SERBP1 partners, 134 proteins (23%) are implicated in mRNA processing, and from this group, 117 participate in mRNA splicing. They include many well-known alternative splicing regulators such as hnRNPU, KHDRBS1, PTBP1, SRSF6, TRA2B, SRSF2,

and hnRNPA1 – **Figure 3A**. In particular, hnRNPU, TRA2B, and KHDRBS1 display high expression correlation with SERBP1 in multiple scenarios – **Table S5**. To determine if SERBP1 expression levels influence splicing, we conducted an RNAseq study in U251 cells. SERBP1 knockdown altered the splicing of 1,625 events (PSI > 0.1, FRD < 0.05) with 70% of them being exon skipping events – **Figure 3B** and **Table S8**. Next, we examined a SERBP1 CLIPseq dataset (36) to search for evidence of SERBP1 direct participation in regulated splicing. From the 1,625 splicing events altered in SERBP1 knockdown cells, CLIP sites were observed close to pertinent splice sites (<100 nucleotides) of 443 (27%) of them - **Figure 3C and Table S8**. SERBP1's association with many known alternative splicing regulators suggests that its impact on regulated splicing requires interaction with other factors. Since hnRNPU was identified as one of SERBP1's main partners and they display strong expression correlation in multiple instances (**Figure 3D**), we decided to conduct additional RNAseq analysis in U251 cells to determine if the two proteins co-regulate splicing events. Circa 30% of the events identified in SERBP1 knockdown cells were also observed upon hnRNPU knockdown, with changes in the same direction – **Figure 3E-F** and **Table S8**.

The results of the splicing analysis also revealed another potential route by which SERBP1 could affect ribosome biogenesis. Most expressed snoRNAs are embedded in introns of protein-coding genes and lncRNAs. Our analysis indicates that SERBP1 knockdown affects splicing events that include introns containing snoRNAs in 13 host genes – **Table S8**.

SERBP1 has a two-way association with PARP1 and PARylation.

We identified important associations between SERBP1 and PARP1, an enzyme that catalyzes the addition of poly(ADP-ribose) (PAR) on target proteins – **Figure 4A**. PARP1 is implicated in DNA repair and regulates multiple stages of gene expression, including transcription, splicing, ribosome biogenesis, and translation (59–61). SERBP1 and PARP1 showed strong expression correlated in several scenarios and similar expression profiles during cortex development – **Figure 4B-C, Table S5**.

Results of high throughput studies established that SERBP1 gets PARylated and binds to PAR (62–64) – **Figure 4D, Table S6**. SERBP1 PARylation by PARP1 was confirmed in an *in vitro* assay – **Figure 4E**. Moreover, we determined that circa 56% of all identified SERBP1 interactors get PARylated and/or bind PAR (**Figure 4F, Table S6**), suggesting that PARylation is an important component in the assembly of protein complexes in which SERBP1 participates. We further investigated SERBP1-PARP1 interaction in 293T and U251 cells in the context of PARP activation. Cell exposure to H_2O_2 enhances PARP1 activity and protein PARylation as shown by Western blots probed with an anti-poly-ADP-ribose binding reagent - **Figure 4G**. In U251 cells, H_2O_2 treatment caused SERBP1 to shift to the nucleus, where it co-localized with PARP1 – **Figure S4A**. Next, we co-transfected SBP-SERBP1-His and Flag-PARP1 in 293T cells and conducted pull-down experiments with streptavidin beads using extracts from cells treated with H_2O_2 and control. An increase in SERBP1-PARP1 interaction was observed in cells treated with H_2O_2 - **Figure 4H**. On the other hand, treatment with the PARP inhibitor PJ34 decreased SERBP1 interaction with PARP1 and G3BP1 as indicated by the results of the pulldown analysis with streptavidin beads - **Figure 4I**. Transgenic SERBP1 expression in 293T cells increased PARylation, as revealed by western blot probed with PAR detecting reagent – **Figure 4J**. To determine if PARylation/PAR binding affects SERBP1 interactions, we transfected 293T cells with an SBP-SERBP1 expressing vector. The experimental group was treated later with PJ34. SERBP1-associated proteins were isolated via pulldown with streptavidin beads and the presence of PARylated proteins was evaluated by Western blot. PARP inhibition decreased the amount of PARylated proteins associated with SERBP1 as shown in the pulldown lanes - **Figure S4B**.

A recently published screening identified genes conferring sensitivity to PARP inhibitors, Olaparib, Rucaparib, and Talazoparib (65). From this study, we generated a list with top hitters

for each drug and compiled the results to identify genes appearing in two or more analyses. The 424 identified genes include SERBP1 and 82 of its interactors - **Table S7**. In agreement, using a proliferation assay, we determined that SERBP1 partial knockdown makes U251 and U343 GBM cells more sensitive to the PARP inhibitor PJ34 – **Figure S4C**.

PARP1 and several of its characterized interactors were determined to be associated with SERBP1 – **Table S1**. Our investigation has determined that the list of PARP1-SERBP1 shared factors is in fact more extensive. A comparison between SERBP1-associated factors and PARP1 interactors detected via proximity labeling (66) identified 199 common factors (including SERBP1 and PARP1), of which about 80% are also PARylated and/or bind PAR (62–64) – **Figure 5A** and **Table S6**. These proteins are implicated in splicing regulation, ribosome biogenesis, and DNA repair – **Figure 5B** and **Table S6**. Among shared SERBP1-PARP1 interactors that get PARylated and/or bind to PAR are multiple key factors implicated in rRNA transcription, processing, and modification, including NOLC1, NOP16, NAT10, DKC1, DDX21, NCL, SMARCA4 and TCOF1 – **Figure 5C and Table S6.** The binding of snoRNAs to PARP1 stimulates its catalytic activity in the nucleolus independent of DNA damage. Activated PARP1 PARylates the RNA helicase DDX21 to promote rDNA transcription (67). DDX21 was identified as a top SERBP1-associated factor, and expression of the two proteins was highly correlated in several scenarios – **Tables S1** and **S5**. Moreover, we and others have determined that SERBP1 preferentially binds snoRNAs, including the ones implicated in PARP1 activation: snoRA37, snoRA74A, and snoRA18 (67). Out of 58 snoRNAs bound by PARP1 (68), 32 of them are also targeted by SERBP1 – **Table S2**.

Adding up to SERBP1-PARP1 strong functional association, we determined that about 50% of SERBP1 interactors known to bind PAR, are also G4 binders – **Figure S5A, Table S6**. Different types of protein domains bind to PAR, including RGG boxes and RRMs (69, 70). These two types of domains are also among the ones that bind G4s. About half of SERBP1-associated proteins that were identified as both PAR and G4 binders contain RGG boxes and/or RRMs (50, 71) – **Figure S5B** and **Table S6**. Based on our findings, we propose the existence of a feedback regulatory model in which SERBP1 influences PARP1 function and PARylation, while PARylation modulates SERBP1 functions and association with its protein partners – **Figure 5D.**

SERBP1 is in association with proteins present in membraneless organelles and Tau aggregates.

GO analysis of SERBP1-associated proteins based on cellular compartment (72) determined that SERBP1 interacts with factors often present in membraneless organelles, including stress granules, P bodies, Cajal bodies, nuclear speckles, paraspeckles, and nucleoli, which suggests SERBP1's likely participation in protein complexes present in these organelles – **Table S9** and **Figure 6**. SERBP1 binding to snoRNAs and scaRNAs further supports its presence in Cajal bodies and nucleolus – **Table S2**. Liquid-liquid phase separation (LLPS) is a main contributor to the formation of membraneless organelles or granules (73). We have previously established that SERBP1 forms biomolecular condensates *in vitro* that are modulated by RNA (25). A characteristic of proteins in LLPS is the presence of IDRs (74, 75). Of all SERBP1-associated proteins present in membraneless organelles, 77% of them contain IDRs – **Table S9**.

SERBP1 has been observed in Tau aggregates in Alzheimer's disease (AD) brains and is part of a group of 261 proteins detected in several studies that examined the composition of Tau aggregates (9). We further investigated SERBP1's association with pathological Tau by co-staining SERBP1 in AD tissues with phospho-tau (Thr231), which is associated with large inclusion and paired helical filaments (PHF) (76). We found a signal overlap between large hyperphosphorylated Tau inclusions and SERBP1 puncta (**Figure 7A**), confirming their close interaction in AD tissue. The interaction between SERBP1 and pTau was confirmed using an *in*

situ proximity ligation assay - **Figure 7B**. Quantification of the PLA signal showed increased SERBP1-pTau interaction in AD compared to Ctr - **Figure 7C**. Western blot analysis showed that SERBP1 displays increased expression in AD brains in comparison to normal controls. Interestingly, SERBP1 appears to be often present as a dimer – **Figure 7D-E**. Overall, our data suggest that SERBP1 shows increased accumulation in AD brains and condenses in hyperphosphorylated Tau aggregates.

146 proteins present in Tau aggregates were also identified as SERBP1 interactors – **Figure 7F** and **Table S9**. GO analysis indicated that this group is strongly associated with ribosome biogenesis, translation, and splicing **- Figure 7F**. snoRNAs are also aberrantly located in Tau aggregates (77). Adding to SERBP1 participation in Tau aggregates, we determined that 66% of the snoRNAs enriched in Tau aggregates were bound by SERBP1 according to our study – **Table S9**. Ribosome biogenesis and translation are impaired in AD (78, 79). SERBP1 may help trap snoRNAs and factors implicated in ribosome biogenesis and translation in Tau aggregates, but further investigation is required.

PARP1 activity is increased in AD brains. Immunostaining of PARP1 and PAR indicates that PARylation is hyperactivated in AD neurons. Ultimately, this hyperactivation can trigger proteins to condense into toxic aggregates that contribute to neurodegeneration (80). We investigated PARP1-SERBP1 association in normal vs. AD brains. PARP1 exhibited a stronger presence in AD cortices compared to controls. Furthermore, PARP1 appeared to co-localize with SERBP1 in the cytoplasmic fraction of AD samples (white arrowhead) – **Figure 8A**. In control samples, PARP1 and SERBP1 also co-localized, albeit to a lesser extent compared to AD samples (confirmed by PCC analysis) – **Figure 8A-B**. Fluorescence profiles corroborate their association – **Figure 8C**. We performed a PLA assay to measure physical interaction between SERBP1 and PARP1. PLA results showed an increased signal for SERBP1/PARP1 association in AD brains in comparison to control brains. This observation was confirmed by the quantification of positive PLA area covered by such association – **Figure 8D**.

G3BP1, a well-established regulator of stress granule assembly, has been identified here as a SERBP1-associated protein – **Table S1**. In AD brains, G3BP1 is present in pathological stress granules (81, 82). Co-immunofluorescence (IF) experiments in control and AD brain sections revealed a stronger fluorescent signal for SERBP1 and G3BP1 in AD compared to controls, indicating higher levels of SERBP1 protein in stress granules in pathological condition – **Figure S6A**. Moreover, SERBP1 IF showed a high density of puncta with some large aggregates in AD samples. To quantify the level of SERBP1 in stress granules in control and AD samples, we measured the number of positive SERBP1 puncta in G3BP1 stress granules, observing a significant increment of SERBP1 in stress granules in AD cases. The total number of G3BP1 and SERBP1 puncta indicated greater accumulation in AD tissues compared to control – **Figure S6B**. SERBP1 and G3BP1 also show strong co-localization in glioblastoma cells and highly correlated expression in different scenarios – **Figure S6C, Table S5**.

DISCUSSION

SERBP1's name relates to its function as a regulator of the gene SERPINE1, which encodes the plasminogen activator inhibitor 1 (PAI-1) (83), a protein implicated in senescence and migration. SERBP1 is localized mostly in the cytoplasm, but it is also present in the nucleus. SERBP1 cytoplasmic/nuclear balance changes during the cell cycle, and its nuclear presence intensifies upon stress (35, 37, 39). We have identified SERBP1's interactome and expanded its regulatory roles – particularly in the nucleus, where it is associated with specific complexes implicated in splicing, cell division, chromosome structure, and different aspects of ribosome biogenesis.

Most SERBP1-associated proteins are also RBPs. However, SERBP1 has unique characteristics; it is mostly disordered and does not display classic RNA binding domains other

than RGG boxes (25). Two commonalities between SERBP1 and its associated proteins are their preference for G4 binding and the fact that they get PARylated and/or bind to PAR. These results indicate that complexes in which SERBP1 participates are assembled via G4 or PAR binding. Since SERBP1 does not display any apparent functional domains and is involved in very distinct regulatory complexes, we suggest that SERBP1 acts in the initial steps of their assembly via recognition of interacting sites in RNA, DNA, and proteins.

SERBP1 in translation regulation and ribosomal biogenesis

SERBP1 interacts with ribosomal proteins and regulates translation (33–36), functioning as a repressor or activator depending on the context. For instance, SERBP1 binding to CtIP mRNA during the S phase increases its translation (35), while changes in binding to the 40S ribosomal subunit during mitosis lead to PKCε pathway-mediated translation repression (36). Additionally, the SERBP1 yeast homolog, STM1, is required for optimal translation under nutritional stress (84). SERBP1 migrates to stress granules under stress conditions (37). Recent findings indicated that translation in these organelles is not uncommon (85), suggesting the possibility of a similar role for SERBP1 as a modulator of translation in stress conditions.

Our GO analyses revealed that SERBP1 interacts with proteins participating in all stages of translation – initiation, elongation, and termination – including both negative and positive regulators. We found that 17% of SERBP1-associated proteins are implicated in translation initiation, including several subunits of the eukaryotic initiation factor 3 (eIF3A-I, L, and M) and CSDE1, among others. These data suggest that SERBP1's primary function in translation regulation lies in initiation. CSDE1 is a known regulator of both cap-dependent and cap-independent translation, functioning either as an enhancer (86, 87) or repressor (88, 89). The expression of CSDE1 is highly correlated with SERBP1 in multiple instances. CSDE1 was proposed to function as a "protein-RNA connector" enabling interactions between RNAs and regulators to control RNA's translational fate (90). A similar role could be ascribed to SERBP1, possibly explaining its different effects on translation.

Multiple SERBP1-associated proteins are involved in viral translation. For instance, the aforementioned interactors, components of the eIF3 complex and CSDE1, are both implicated in IRES-mediated viral translation in a variety of viruses (91–93). SERBP1 itself has also recently been shown to interact with dengue virus RNA and regulate its translation (94). Finally, we observed a significant overlap between SERBP1-associated proteins and the SARS-CoV-2 interactome, with 82 proteins out of 145 shared interactors being involved in translation.

SERBP1's interactors and its presence in the nucleolus suggest its participation in ribosome biogenesis. Besides binding to mRNA, SERBP1 binds to rRNA and snoRNAs, which play a role in pre-rRNA processing and modification (95). SERBP1, and 98 of its associated proteins, were previously identified in a screening for factors affecting rRNA processing (96). SERBP1's binding profile to rRNA and snoRNA is dynamic, as shown by differences in iCLIP sites in mitotic vs. asynchronous cells (36), hinting that SERBP1's participation in these processes is cell cycle-dependent as seen for translation. FBL, a SERBP1-associated protein, is involved in pre-rRNA processing, pre-rRNA methylation, and ribosome assembly (97). Recently, it has been shown that FBL also modulates rDNA transcription during the cell cycle according to its acetylation status, leading to higher levels of rRNA synthesis in interphase and lower levels during mitosis (98). SERBP1 also interacts with multiple proteins of the cohesin complex (SMC1, SMC3, and PDS5B) plus the associated factor, CTCF. Cohesin forms an enhancer boundary complex who's binding upstream of the 47S rDNA is as an early event in the activation of rDNA transcription (99). In accordance with this finding, mutations in cohesin components have been linked to defects in both rRNA production and processing in yeast and human cells (100). Two of SERBP1's top interactors, the RNA helicase DDX21 and NCL, also promote rDNA transcription (101, 102)

Overall, these findings indicate a rather fluid role for SERBP1 in translation regulation, promoting or repressing different translational steps and acting in rRNA processing/modification and ribosome biogenesis through diverse pathways.

SERBP1 and PARylation

PARylation of SERBP1 was described in several different studies (62, 63, 103–106). Moreover, the expression of human PARP1 in *S. cerevisae,* which does not naturally express PARP proteins, caused PARylation of many proteins implicated in ribosomal biogenesis, including STM1, SERBP1 homolog (107). Our results suggest a two-way association between SERBP1 and PARP1. First, SERBP1 and 56% of its identified associated proteins either get PARylated and/or bind PAR (62–64). This result suggests that SERBP1 participates in several regulatory complexes modulated via PARylation.

PARylation of RBPs ultimately influences RNA processing and expression (59, 108). In particular, PARylation of splicing regulators is known to affect alternative splicing. For instance, PARylation of HRP38's RNA binding domain decreases its binding activity and subsequently its ability to inhibit splicing (59). PARylation also affects protein-protein interaction as observed in the case of hnRNPA1 (109). Finally, PARP1 itself is involved in splicing. PARP1 binds RNA with a preference for intronic regions, while its knockdown affected many splicing events (110). Several splicing regulators known to get PARylated and/or bind to PAR were identified as SERBP1-associated proteins, including hnRNPs (A1, H1, A2B1, H3, K, I, and U) and SR proteins (SRSF2, SRSF3, and SRSF9). In particular, most splicing alterations observed in SERBP1 KD cells were also present upon hnRNPU KD, suggesting that they work as co-factors in splicing regulation. Altogether, the data suggest that SERBP1 is directly implicated in splicing regulation and is present in complexes modulated by PARylation.

PAR induces phase separation of proteins containing IDRs and the formation of molecular condensates or membraneless organelles such as stress granules, mitotic spindles, DNA repair foci, and nucleoli (111). Similarly, ADP-ribose can be conjugated to polar and charged amino acids, which are often found in IDRs (111). Ultimately, PAR serves as a scaffold to assemble protein complexes in different contexts where PAR length and structure influence their composition (111). The large number of PARylated proteins and PAR binders found among SERBP1-associated proteins strongly indicates that PAR is a critical component of the regulatory complex in which SERBP1 participates, especially in membraneless organelles. As a protein that interacts with PARP1, promotes PARP activity, gets PARylated, and binds PAR, we suggest that SERBP1 acts as a critical factor in the assembly of PARylation-dependent complexes. Additional analyses are required to assess whether the formation of such complexes depends on SERBP1 and if inhibition of SERBP1 PAR binding activity could be explored as a therapeutic strategy.

SERBP1 exhibited a punctate distribution in normal brain, indicating its presence as functional singlet condensate. However, in AD brain tissues, SERBP1 appeared to accumulate in large cytoplasmic aggregates and to strongly co-localize with PARP1. This result suggests that PARP1 modulates liquid-liquid phase separation (LLPS) and a PARylation-mediated mechanism is likely involved in SERBP1's pathological transition from condensate to aggregate. Several RBPs containing intrinsically disordered regions, like SERBP1, have been shown to display alterations in LLPS in neurodegenerative diseases (112, 113).

SERBP1 and G4 binders

SERBP1 belongs to a group of neuronal-related RBPs that share structural characteristics and preferentially bind to G quadruplexes (G4s). G4s are complex DNA or RNA structures that display stacked tetrads of guanosines stabilized by Hoogsteen base pairing. rG4s function as regulatory elements in different stages of gene expression, including splicing, mRNA decay,

polyadenylation, and translation. G4s have been linked to cancer, viral replication, and in particular neurodegenerative diseases and neurological disorders (114–116).

The SERBP1 interactome shows an interesting parallel between PAR and G4 binding. Almost half of the SERBP1-associated proteins that bind G4 also bind PAR. PAR and G4s occupy the same regulatory space that includes DNA repair and stress response, and both induce phase separation. However, not much is known regarding the association between G-quadruplex and PAR binding/PARylation, aside from the fact that PARP1 binds G4s, and this leads to the activation of its enzymatic activity (117). We envision two possible scenarios for SERBP1 and its associated proteins. Two types of domains have been implicated in both PAR and G4 binding, RGG boxes and RRMs. Among 105 SERBP1-associated factors that bind PAR and G4, 51 contain RGG and/or RRM domains. Proteins that employ the same domain to bind PAR and G4 could transit from G4 to PAR binding complexes, depending on the cellular state. In a different setting, binding to G4 motifs in DNA or RNA could serve as a starting point for the assembly of PAR binding/PARylated protein complexes. Further investigation on PAR- and G4-dependent interactions and identification of G4 and PAR binding domains in proteins present in these complexes are needed to elucidate the relationship between PAR and G4 binding.

SERBP1 potential role in neurodegenerative diseases and neurological disorders

SERBP1 expression in the brain is lower than in other organs and is increased in glioblastoma (26) and Alzheimer's brains, as shown in this study. SERBP1 is present in Tau aggregates (9) and in pathological stress granules in connection with G3BP1. PAR levels regulate the dynamics of RNPs and aberrant PARP1 activity promotes aggregation (109). Over 60% of SERBP1-associated proteins detected in Tau aggregates get PARylated and/or bind PAR (62–64) and increased SERBP1-PARP1 interaction was observed in AD brains. Besides its potential role in aggregate formation, increased expression of SERBP1 in Alzheimer's brains could lead to important changes in gene expression. SERBP1 is highly expressed in neuronal and glioma stem cells and its levels drop significantly during neurogenesis. SERBP1 transgenic expression disrupted neuronal differentiation while its knockdown increased the expression of genes implicated in nervous system development, synaptic signaling, organization, memory, learning, and behavior (26).

SERBP1-associated proteins contain several factors involved in neurological disorders and neurodegenerative diseases, including FMR1, SMN1, and PABPN1. SERBP1 interaction with FMRP (FMR1) has been previously described (36, 37). Not only was this interaction validated, but we also determined that SERBP1 associates with FMRP partner proteins FXR1 and FXR2. FMRP is the main driver of Fragile X mental retardation but has also been linked to Alzheimer's disease and autism (118, 119). FMRP is a complex protein that binds different RNA motifs (including G4s) and regulates translation, splicing, RNA editing, and miRNA function, affecting synapse formation and plasticity, stress granule formation, channel signaling, and differentiation (120–123). Previous results indicate that SERBP1 and FMRP interact in different contexts (36, 37), suggesting that they function together in diverse stages of gene expression.

Spinal Muscular Atrophy (SMA) is caused by mutations in the SMN1 gene. Patients show progressive lower motor neuron loss (6). We observed associations between SERBP1, SMN1, and other members of the SMN complex, GEMIN4 and 5. SMN1 brings together the complex and is essential for spliceosome assembly. Since motor neurons are particularly sensitive to SMN1 mutations, additional roles for the SMN complex in these cells are proposed (6).

SYNCRIP and hnRNPU were identified among the top proteins associated with SERBP1 based on our proteomics analyses and gene expression correlations. SYNCRIP plays multiple roles in neuronal cells, including dendritic translation, synaptic plasticity, axonogenesis, and morphology (124–128). hnRNPU has been implicated in cortex development (129). Mutations in both hnRNPU and SYNCRIP are linked to intellectual disability (130–132) and

neurodevelopmental disorders (133, 134), and were the two top candidates in an IBM Watson-based study to identify RBPs altered in amyotrophic lateral sclerosis (ALS) (135).

SERBP1 has not been studied in the context of the nervous system, and its contribution to neurodegenerative diseases and neurological disorders remains to be investigated. Our results suggest that SERBP1 is “guilty by association” as it interacts with several RBPs that function as key players in these scenarios. Moreover, SERBP1 regulates the expression of genes implicated in neuronal differentiation and synaptogenesis, processes often compromised in disease states. In the case of Alzheimer’s disease, increased expression of SERBP1 and its presence in pathological aggregates hint at a potential involvement. Additional studies are necessary to establish causal connections that link SERBP1 to AD phenotypes.

MATERIAL AND METHODS

Cell culture, transfection, knockdown

U251 and U343 glioblastoma cell lines were obtained from Uppsala University (Uppsala, Sweden). 293T cells were obtained from the American Type Tissue Collection (ATCC). All cell lines were cultured in DMEM medium (HyClone, Cat# SH30243.01) supplemented with 10% FBS (Corning, Cat# 35015CV) and 1% penicillin/streptomycin (Gibco, Cat# 10378016). Cells were maintained at 37 °C in a 5% CO_2 atmosphere. Cell lines were confirmed to be correct using Short Tandem Repeat profiling. They were regularly tested for mycoplasma contamination

Knockdown of SERBP1 (siSERBP1 KD) in U251 and U343 cells was performed by reverse transfection with 25 nM of control or SERBP1 SMARTpool siRNA (Dharmacon, Cat# L-020528-01-0005) using Lipofectamine RNAiMAX (Invitrogen, Cat# 13778150).

Plasmid constructs

A vector containing the Streptavidin-Binding Peptide (SBP)-Tag was prepared in pEF1 (Thermo Fisher, Cat# V 92120), and SERBP1 ORF was cloned in frame with the His-Myc-tag present in the vector to create pSBP-SERBP1. The SBP-tag contains 38 amino acids and binds to streptavidin with an equilibrium dissociation constant of 2.5 nM (136). Ultra-SERBP1 lentiviral vector (26) was used as a control in pulldown experiments. SERBP1 ORF was inserted into the pcDNA3.1-mGreenLantern plasmid (Addgene Plasmid #161912) to make mGreen-SERBP1. Flag-PARP1 was obtained from Addgene (#111575).

Primer name	sequence
SERBP1_for_ EcoRI	tatagaattcATGCCTGGGCACTTAATGCCTGGGCACTTA
SERBP1_rev_XbaI	tatatctagaAGCCAGAGCTGGGA
mGL_SERBP1_BsrGI	actgtacaagATGCCTGGGCACTTACAG
mGL_SERBP1_XbaI	atctagattaAGCCAGAGCTGGGAA

Identification of SERBP1 interactors

293T cells were seeded (triplicate) in 10 cm dishes the day before transfection. pSBP-SERBP1 or pUltra-SERBP1(control) plasmids were transfected using $CaCl_2$. 48 hours later, cells were collected and washed twice in cold PBS. Total protein extract was prepared by using TNE buffer (Tris pH 7.4 10 mM, NP-40 1%, NaCl 150 mM, and phosphatase inhibitor cocktails, Thermo Fisher Scientific, Cat #78430), incubating cells for 30 minutes on ice, and then sonicating five times for 3 seconds at 20% amplitude and 10-second intervals. A second batch of samples was prepared by using polysomal lysis buffer (KCl 100 mM, EDTA 25 mM, $MgCl_2$ 5 mM, HEPES pH 7.0 10 mM, NP-40 0.5%, DTT 2 mM, VRC 0.4 mM, glycerol 10%, and phosphatase inhibitor cocktails, Thermo Fisher Scientific). Cell lysates were centrifuged at 4°C to eliminate debris and supernatants were collected and used later in pulldown assays.

50 µl of packed streptavidin beads (GE Healthcare Life Sciences, Cat# 17-5113-01) were washed two times in PBS and subsequently blocked in 1% BSA/PBS for 30 minutes at 4°C. Beads were finally washed five times in TNE buffer and then combined with cell extracts. The solution was incubated at room temperature for 2 hours and beads were later recovered via centrifugation at 4°C. The supernatant was discarded, and beads were washed five times with 1 ml of TNE buffer. To elute proteins, samples were resuspended in elution buffer (Tris pH 7.4 50 mM, NaCl 250 mM, NP-40 0.5%, deoxycholate 0.1%, 10 mM biotin), mixed, and incubated for 45 min at 37°C in a thermo-shaker. The supernatant was collected after centrifugation for mass spectrometry analysis.

Protein identification by mass spectrometry

Analysis of proteins associated with SERBP1. Proteins were separated by 1D SDS-PAGE using a Criterion XT 12% gel that was electrophoresed for ~1.5 cm and then stained with Coomassie blue (one experiment per gel). The protein-containing region of each gel lane was divided into six slices which were individually reduced *in situ* with TCEP [tris(2-carboxyethyl)phosphine] and alkylated in the dark with iodoacetamide prior to treatment with trypsin. Each digest was analyzed by capillary HPLC-electrospray ionization tandem mass spectrometry on a Thermo Scientific Orbitrap Fusion Lumos mass spectrometer. On-line HPLC separation was accomplished with an RSLC NANO HPLC system (Thermo Scientific/Dionex): column, PicoFrit™ (New Objective; 75 µm i.d.) packed to 15 cm with C18 adsorbent (Vydac; 218MS 5 µm, 300 Å). Precursor ions were acquired in the Orbitrap mass spectrometer in centroid mode at 120,000 resolution (*m/z* 200); data-dependent higher-energy C-trap dissociation (HCD) spectra were acquired at the same time in the linear trap using the “top speed” option (30% normalized collision energy). Mascot (v2.7.0; Matrix Science) was used to search the spectra against a combination of the human subset of the UniProt database plus a database of common contaminants [UniProt_Human 20181204 (95,936 sequences; 38,067,061 residues)]; contaminants 20120713 (247 sequences; 128,130 residues)]. Subset search of the identified proteins by X! Tandem, cross-correlation with the Mascot results, and determination of protein and peptide identity probabilities were accomplished by Scaffold (v4.9.0; Proteome Software). The thresholds for acceptance of peptide and protein assignments in Scaffold were set to yield < 1% protein FDR. Corresponding UniProt IDs for the proteins were obtained using the UniProt ID mapping service (71).

Western blots

Cells. Cells were harvested and lysed in Laemmli sample buffer (BioRad, Cat# 1610737). Cell extracts were separated on an SDS-PAGE gel, and transferred to PVDF membranes, previously activated with methanol. Membranes were blocked in 5% milk Tris-buffered saline with Tween 20 and probed with a collection of different antibodies listed below. Horseradish peroxidase (HRP)-conjugated goat anti-rabbit antibody (Santa Cruz Biotechnology, Cat# sc-2030) or HRP-conjugated goat anti-mouse (Santa Cruz Biotechnology, Cat# sc-2005) were used as secondary antibodies. Immobilon Western chemo-luminescence substrate (Millipore, Cat# WBKLS0500) was used to detect selected proteins.

Human samples. Western blots were performed with proteins extracted from control and Alzheimer’s brains. Approximately 10 µg of protein were loaded into precast NuPAGE 4-12% Bis-Tris gels (Invitrogen) for analysis by sodium dodecyl sulfate–polyacrylamide gel electrophoresis. The separated proteins were subsequently transferred onto nitrocellulose membranes and blocked overnight at 4°C with 10% nonfat dry milk. The membranes were then probed for 1 hour at room temperature with primary antibodies - anti-SERBP1 (1:100, sc100800) and anti-glyceraldehyde 3-phosphate dehydrogenase (GAPDH) (1:1000, ab9485, Abcam) - diluted in 5% nonfat dry milk. SERBP1 immunoreactivity was detected with a horseradish peroxidase–conjugated anti-mouse IgG (1:5000, GE Healthcare). GAPDH

immunoreactivity was detected using an anti-mouse IgG (1:6000, GE Healthcare) diluted in 5% nonfat dry milk. An enhanced chemiluminescence reagent (ECL Plus, Amersham) was used to visualize the bands. The amount of protein was normalized and quantified using the loading control GAPDH.

Antibodies

anti-SERBP1 (Santa Cruz Biotechnology, Cat# SC100800), anti-G3BP1 (Cell Signaling, Cat# 17798S), anti-PARP1 (Cell Signaling, Cat# 9532S), anti-SYNCRIP (Invitrogen, Cat# PA5-59501), anti-hnRNPU (Cell Signaling, Cat# 34095), anti-Puromycin (Kerafast, Cat# EQ0001), anti-His (Santa Cruz Biotechnology, Cat# sc-53073), anti-Flag (Invitrogen, Cat# MA1-91878), anti-GAPDH (Santa Cruz Biotechnology, Cat# SC32233), anti-β-Actin (Abcam, Cat# ab8227), anti-β-Tubulin (Sigma-Aldrich, Cat# T8328), anti-α-Tubulin (Invitrogen, Cat# 236-10501), FBL (Cell Signaling, Cat# C13C3), NCL (Cell Signaling, Cat# D4C70).

High-throughput drug screening

High-throughput screening was conducted with the Cambridge Cancer Compound Library (Selleck Chem, Cat# L2300) of 293 compounds of interest (Table S7). All compounds dissolved in DMSO to a stock concentration of 10mM and further diluted in PBS to achieve a final treatment concentration of 100 nM and a final DMSO concentration of 0.1%. Four replicates of both U343 OE and U343 Control cells were plated in 384 well white polystyrene microplates (Thermo Scientific) at a seeding density of 5.0 x 103 cells/well 12 hours before treatment. Cell seeding and treatment was conducted by an automated electronic pipetting system to increase pipetting accuracy and to minimize variability between replicates (Integra VIAFLO 384). After 24 hours of treatment, cells were incubated with Cell Titer Glo 2.0 (Promega, Cat# G9243) according to the manufacturer's protocol. The addition of the reagent lyses cells and attaches a luminescent tag to ATP molecules in order to assess cell viability. Within 10 minutes of Cell Titer Glo 2.0 reagent addition, ATP measurements were then collected as luminescence intensities by a Tecan Spark microplate reader. Dixon's Q test was used to eliminate outliers prior to statistical analysis. Experimental ATP intensities were normalized to respective vehicle controls to assess cell viability following drug treatment. Student's Ttest was used to evaluate significant differences between reactions of U343 and U343 SERBP1 OE to each treatment.

Puromycin assays

siSERBP1 KD in U251 and U343 cells was performed as described above. 72 hours after transfection, cells were incubated with 10 µg/ml Puromycin (Sigma-Aldrich, Cat# P7255) for 15 minutes at 37 °C and 5% CO_2. Cells were then placed on ice and washed twice with cold PBS before being harvested in Laemmli sample buffer. Western blots were performed as described above with 15 µg protein extracts.

Protein co-localization

U251 cells were cultured on glass coverslips until 80% confluent and fixed in 4% paraformaldehyde followed by permeabilization with 0.1% TritonX-100 for 2 minutes. Cells were then stained with primary antibody for 1 hour followed by the secondary antibody conjugated to Alexa Fluor 488 or 568 (Invitrogen, Invitrogen, Cat# A11004 and A11008). After washing with PBS, cells were stained with DAPI and mounted onto glass slides with FluorSave (Invitrogen, Cat# 345789) before being analyzed by fluorescence microscopy.

Impact of SERBP1 on cell division

24 hours after siSERBP1 KD in U251 and U343, cells were exposed to 20 nM of Paclitaxel (Cayman Chem, Cat# 10461) for 24 hours. Cells were fixed in 4% PFA and stained with α-

Tubulin and DAPI. The experiment was performed in triplicates and 1000 cells were counted per replicate. Statistical significance was evaluated by Student's t-test.

In vitro PARylation assay

Flag-tagged PARP1 was expressed in insect cells and purified as previously described (137). 6xHis-tagged SERBP1 was purified as in (25). Briefly, purified recombinant PARP1 (0.1 µM) and SERBP1 (0.6 µM) were combined in an ADP-ribosylation reaction (20 µL) with or without sheared salmon sperm DNA (sssDNA) (100 ng/µL) and NAD^+ (100 µM). The reactions were incubated at room temperature for 15 minutes. The reaction products were analyzed on 8% PAGE-SDS gels with silver staining or Western blotting for PAR using a recombinant anti-poly-ADP-ribose binding reagent (Millipore, Cat# MABE1031; RRID: AB_2665467).

SERBP1 impact on PARylation

pcDNA3.1-EF1a-mGreenLantern-SERBP1 or control plasmid pcDNA3.1-EF1a-mGreenLantern was transfected into 293T cells. 48 hours later, cells were collected and lysed in Laemmli sample buffer. 10 µg of extracted proteins were separated on SDS-PAGE gel and Western blot was performed as described. Poly-ADP-ribose binding reagent (Sigma-Aldrich, Cat# MABE1031) was used to detect oligo- and poly-ADP-ribosylated (PARylated) proteins.

Sensitivity to PARP inhibitor

U251 and U343 siSERBP1 knockdown was performed as described above. 5 µM of PARP inhibitor PJ34 (Enzo, Cat# ALX-270-289) was used to treat the cells 24 hours later. The Essen Bioscience IncuCyte automated microscope system was used to follow the proliferation of U251 and U343 glioblastoma cells over 150 hours. Differences in proliferation between single and combined treatment at 100 or 150 hours were analyzed graphically. Statistical significance was calculated by Student's t-test and the combination treatment was evaluated with the Combination Index (138).

Immunolabeling of fixed human brain sections

Frozen cortical sections were first fixed in chilled 20% methanol. To eliminate autofluorescence from lipofuscin, we incubated the sections with TrueBlack® Lipofuscin Autofluorescence Quencher (#23007, Biotium) for 10 minutes at room temperature. After three washes with ethanol 70%, the sections were permeabilized in PBS/0.4% Triton-X100 for 5 minutes. After 1 hour of blocking in PBS/10% NGS/0.2% Triton at room temperature, the sections were incubated in primary antibodies diluted in PBS/10% NGS overnight at 4°C. Immunolabeling for G3BP1 (5 µg/ml, 2F3, Abcam Cat# ab56574), Phospho-Tau (Thr231) (1:500, AT180, Thermo Fisher Scientific #MN1040) and SERBP1 (1:50, 1B9, Santa Cruz Bio Cat# sc-100800) was performed in all control (N=3) and AD (N=3, Braak Stage V-VI) human brains. The next day, sections were washed three times in PBS (5 minutes each), and secondary antibodies were applied for 45 minutes: Alexa Fluor 488 and 568 (1:200, Life Technologies). After further washing in PBS, slides were then mounted with Prolong Gold Antifade with DAPI (Thermo Fisher Scientific Cat# P36931) to stain the nuclei. Granule density of G3BP1 and SERBP1 were measured in 3 Ctr and 3 AD cases, and images in triplicate from each case were analyzed by ImageJ FIJI (NIH) software. SERBP1 associated with stress granules was measured as the ratio between colocalizing SERBP1/G3BP1 puncta and G3BP1 total granules in the cortical section using ImageJ FIJI (NIH) software.

Human tissue harvesting

Frontal cortices of frozen brain tissues from age-matched control subjects (N=6), AD cases (N=6) were received as frozen blocks from the Institute for Brain Aging and Dementia at UC Irvine, approved by the Institutional Ethics Committee. Brain tissues were homogenized in 1X

PBS mixed with a protease inhibitor cocktail (Roche) and phosphatase inhibitor (Sigma) at 1:3 (w/v) dilution of brain: PBS. Samples were then centrifuged at 10000 rpm for 20 min at 4°C. The supernatants, PBS-soluble fractions were aliquoted, snap-frozen, and stored at −80°C until use. The pellets were resuspended in the homogenization buffer (1X PBS) and were considered as insoluble fractions. They were also aliquoted and frozen at -80°C until use. Brain tissues analyzed in this study from diseased and age-matched non-demented control subjects are listed in Table 1.

Proximity ligation assay (PLA)

Detection of protein-protein interactions was conducted by an in-situ proximity ligation assay. The method depends on the recognition of target molecules in close proximity (<40 nm) by pairs of affinity probes, giving rise to an amplifiable detection signal. Briefly, PLA in mouse brain tissue has been performed using Duolink® PLA in Situ Red starter kit mouse/rabbit (Sigma Aldrich, DUO92101). The staining was performed following each protocol passage without modifications. Time of incubation and concentration of antibodies is established from IF protocol. Primary antibodies used for in situ proximity assay were: SERBP1 (1:100), PARP1 (1:200), and pThr231-Tau (1:500). Amplified red signal has been detected using Keyence Microscope.

Venn diagram statistics

Venn diagrams were created using online software (https://bioinforx.com/apps/venn.php). P-values for overlaps between two groups were calculated with a separate online tool (http://nemates.org/MA/progs/overlap_stats.html).

Gene ontology and network analyses

Gene Ontology (GO) enrichment analyses were performed using ShinyGO (versions 0.67 and 0.77), Metascape (version 3.5), and Panther (version 17.0) (27, 28, 72). Associations between GO terms were established using Revigo (29). Network analyses were conducted using STRING (version 11.5) and Metascape (28, 139) and visualized using Cytoscape (version 3.9.1) (140).

Expression correlation analyses

We performed expression correlation analyses using resources in R2 (http://r2.amc.nl) to identify genes with a strong positive correlation with SERBP1 ($R \geq 0.3$, p-value ≤ 0.05, Pearson correlation) in the TCGA glioblastoma set (RNA-Seq samples), sarcoma (TCGA), bladder urothelial carcinoma (TCGA), neuroblastoma (SEQC), pancreatic adenocarcinoma (TCGA), and normal brain (Hardy, $R \geq 0.5$ was selected in this case due to the high number of correlated genes). Additional analyses were conducted using the Ivy GAP glioblastoma dataset (141) following their default parameters ($R \geq 0.3$).

The Cortecon resource (142) was used to identify genes that share similarity with SERBP1 regarding their expression profile during *in vitro* cortex development. SERBP1 is part of cluster 5 which is linked to pluripotency. Genes that were in clusters related to pluripotency and whose overall profile resembles cluster 5 were selected for further analyses.

Identification of protein features and domain

Pfam accession numbers were obtained using the UniProt ID mapping service (71). R code was used to count the frequency of each accession number and create the consolidated data with fold enrichment and fdr-values. All accession numbers with a count above the average were analyzed with the dcGO Enrichment mining service (143).

Databases and datasets used for characterization of SERBP1-associated proteins

STM1 interactors were downloaded from BioGRID (version 4.4) (32) and human orthologs were obtained using the WORMHOLE website (144). Proximity-dependent biotinylation (Bio-ID) data for SERBP1 were taken from (30, 31). Proteins of the SARS-CoV-RNA interactome were derived from (57) and those of the PARP1 interactome from (66). RGG box-containing proteins were obtained from (50), and RRM motif-containing proteins from UniProt (71). G4 binding proteins were extracted from (46, 47), PAR binding proteins were obtained from (64), and PARylated proteins were identified by high-throughput studies described in (62, 63). The MobiDB database (version 5.0) (45) was used for identifying IDR-containing proteins. Data on the Tau aggregate interactome were derived from different studies compiled by (9).

Splicing analyses

To identify splicing alterations induced by SERBP1 and hnRNPU knockdown, adapter sequences were first trimmed from raw RNA-Seq reads of control and knockdown samples (26). RNA-Seq reads were then aligned against the human reference genome (version GRCh38) (145) and matching GENCODE transcriptome (v29) (146) using STAR (default parameters; version 2.7.7.a) (147). High-quality mapped reads ($q > 20$) from control and knockdown samples were processed using rMATS (default parameters; version v4.1.2) (148) to characterize splicing events. Events were classified into exon skipping (SE), mutually exclusive exons (MXE), intron retention (RI), alternative donor site (A5SS) or alternative acceptor site (A3SS). Splicing events were considered significant if their FDR-adjusted p-values were below 0.05 and absolute delta Percent Splice Inclusion (deltaPSI) above 0.1. Sashimi plots of splicing events were created using the rmats2sashimiplot tool (https://github.com/Xinglab/rmats2sashimiplot). To assess SERBP1 binding to the identified splicing alterations, we obtained processed iCLIP data from (36). The presence of iCLIP sites in the splicing alterations induced by SERBP1 knockdown was evaluated considering a window of 100 nt around splicing events using the bedtools intersect software (149).

Identification of snoRNAs and scaRNAs bound by SERBP1.

RIP-sequencing results for SERBP1 were obtained from (26). Sequencing reads were processed using Kallisto (default parameters, version 0.46.1) (150) with an index of 31 k-mers and GENCODE (v28) as the reference for the human transcriptome (146). Transcript abundance estimates were then collapsed into gene-level counts using the R package tximport (151). Differential gene expression analyses were performed using DESeq2 (152). We compared SBP-SERBP1 versus SBP-GST samples and used log2 fold change ≥ 0.5 and adjusted (false discovery rate, FDR) p-value < 0.05 to identify snoRNAs and scaRNAs preferentially associated with SERBP1.

DATA AVAILABILITY

The mass spectrometry datasets generated and analyzed during this study are available in the MassIVE repository as a partner with ProteomeXchange and can be accessed by:
(1) MassIVE dataset identifier MSV000091749, ftp://massive.ucsd.edu/v05/MSV000091749/, ProteomeXchange dataset identifier PXD041664
(2) MassIVE dataset identifier MSV000093355, ftp://massive.ucsd.edu/v06/MSV000093355/, ProteomeXchange dataset identifier PXD046851

RNAseq datasets are available at the European Nucleotide Archive (ENA) with the accession number PRJEB69681.

The following datasets were generated:

HOSPITAL SIRIO LIBANES. Raw sequencing data for RNAseq study in U251 cells (control vs. SERBP1 KD and control vs. hnRNPU KD). PRJEB69681.
https://www.ebi.ac.uk/ena/browser/view/PRJEB69681

Susan Weintraub. MassIVE MSV000091749 and MassIVE MSV000093355. Raw Mass spectrometry data for pulldown study (control vs. SERBP1) in 293T cells to identify proteins associated with SERBP1.
https://massive.ucsd.edu/ProteoSAFe/dataset.jsp?task=a20a200385114896be5854646c2149d
https://massive.ucsd.edu/ProteoSAFe/dataset.jsp?task=a775aabf74874af784b475db3a02c609

Code to perform the analysis of SERBP1 impact on splicing can be found in the Open Science Framework: DOI 10.17605/OSF.IO/4EHZS

The following previously published data sets were used:
Youn, J. Y., Dunham, W. H., Hong, S. J., Knight, J. D. R., Bashkurov, M., Chen, G. I., Bagci, H., Rathod, B., MacLeod, G., Eng, S. W. M., Angers, S., Morris, Q., Fabian, M., Côté, J. F., & Gingras, A. C. (2018). High-Density Proximity Mapping Reveals the Subcellular Organization of mRNA-Associated Granules and Bodies; High-Confidence BioID Proximity Interactome for the Organization of RNA Biology. IDs (three sets) MSV00008141, MSV000081412, MSV000081413. In the public domain at MassIVE Repository https://massive.ucsd.edu/.
https://massive.ucsd.edu/ProteoSAFe/dataset.jsp?task=3d92815a96454ea2a13e7f147ec2b09e
https://massive.ucsd.edu/ProteoSAFe/dataset.jsp?task=e774f511588c4e109aba6d76a6ee264a
https://massive.ucsd.edu/ProteoSAFe/dataset.jsp?task=db890fe0ae804b0592d162a07894f2f0.

Go, C. D., Knight, J. D. R., Rajasekharan, A., Rathod, B., Hesketh, G. G., Abe, K. T., Youn, J. Y., Samavarchi-Tehrani, P., Zhang, H., Zhu, L. Y., Popiel, E., Lambert, J. P., Coyaud, É., Cheung, S. W. T., Rajendran, D., Wong, C. J., Antonicka, H., Pelletier, L., Palazzo, A. F., Shoubridge, E. A., … Gingras, A. C. (2021). A proximity-dependent biotinylation map of a human cell; Mass spectrometry samples and results for the core BioID dataset. IDs (two sets) MSV000084359, MSV000084360. In the public domain at MassIVE Repository https://massive.ucsd.edu/.
https://massive.ucsd.edu/ProteoSAFe/dataset.jsp?task=2749913f600246d5907d344007def7ae,
https://massive.ucsd.edu/ProteoSAFe/dataset.jsp?task=bd7ca8514fee41da806cf16babecc35b.

HOSPITAL SIRIO LIBANES. RNA sequencing of U251 SERBP1 knockdown cells and RIP sequencing for the identification of SERBP1 targets in 293T cells. PRJEB35774. https://www.ebi.ac.uk/ena/browser/view/PRJEB35774

Lee, S., Lee, Y. S., Choi, Y., Son, A., Park, Y., Lee, K. M., Kim, J., Kim, J. S., & Kim, V. N. (2021). Profile of the SARS-CoV-2 RNA interactome. PXD024808. https://proteomecentral.proteomexchange.org/cgi/GetDataset?ID=PXD024808.

Mosler, T., Baymaz, H. I., Gräf, J. F., Mikicic, I., Blattner, G., Bartlett, E., Ostermaier, M., Piccinno, R., Yang, J., Voigt, A., Gatti, M., Pellegrino, S., Altmeyer, M., Luck, K., Ahel, I., Roukos, V., & Beli, P. (2022). PARP1 proximity proteomics reveals interaction partners at stressed replication forks. PXD037154. https://proteomecentral.proteomexchange.org/cgi/GetDataset?ID=PXD037154.

Herviou, P., Le Bras, M., Dumas, L., Hieblot, C., Gilhodes, J., Cioci, G., Hugnot, J. P., Ameadan, A., Guillonneau, F., Dassi, E., Cammas, A., & Millevoi, S. (2020). hnRNP H/F drive

RNA G-quadruplex-mediated translation linked to genomic instability and therapy resistance in glioblastoma. PXD015609. https://www.ebi.ac.uk/pride/archive?keyword=PXD015609.

Jernej Ule, Peter Parker. SERBP1 iCLIP in mitotic and asynchronous cells with Blu577 treatment. E-MTAB-10830. https://www.ebi.ac.uk/biostudies/arrayexpress/studies/E-MTAB-10830

FUNDING

This work was supported by the Cancer Prevention and Research Institute of Texas [RP200595 to LP], Alzheimer's Association [AARGD-NTF-22-968603 to LP] and a Mays Cancer Center Pilot Grant [to LP]. PAFG was supported by grants from Serrapilheira Foundation and Fundação de Amparo à Pesquisa do Estado de São Paulo (FAPESP) [2018/15579-8]. MM was sponsored by the Alzheimer's Association [AARF-21-720991]. GDAG was supported by a fellowship from FAPESP [2017/19541-2] and Young Scientist program, Hospital Sírio-Libanês. KB and ML were sponsored by the The German Academic Exchange Service (DAAD). AK was supported by NIH Supplement 2R01 HG006015 and the Greehey Foundation. AB was partially supported by a Voelker Fund Young Investigator Grant to DSL.

CONFLICT OF INTEREST

The authors declare no competing interests.

ACKNOWLEDGEMENTS

Mass spectrometry analyses were conducted at the Institutional Mass Spectrometry Laboratory, University of Texas Health Science Center, supported in part by NIH grant P30 CA54174-23 (S.T. Weintraub, Mays Cancer Center Mass Spectrometry Shared Resource) and the University of Texas System Proteomics Core Network for purchase of the Orbitrap Fusion Lumos mass spectrometer, with expert technical assistance of Sammy Pardo and Dana Molleur. We would like to thank Dr. Jernej Ule and Dr. Rupert Faraway for sharing the SERBP1 CLIP data and their valuable input. The authors would like to acknowledge Karen Klein for excellent editorial service.

REFERENCES

1. Gerstberger,S., Hafner,M. and Tuschl,T. (2014) A census of human RNA-binding proteins. *Nat Rev Genet*, 15, 829–845. doi: 10.1038/nrg3813.

2. Corley,M., Burns,M.C. and Yeo,G.W. (2020) How RNA-binding proteins interact with RNA: molecules and mechanisms. *Mol Cell*, 78, 9–29. doi: 10.1016/j.molcel.2020.03.011.

3. Kelaini,S., Chan,C., Cornelius,V.A. and Margariti,A. (2021) RNA-binding proteins hold key roles in function, dysfunction, and disease. *Biology (Basel)*, 10, 366. doi: 10.3390/biology10050366.

4. Chan,J.N., Sánchez-Vidaña,D.I., Anoopkumar-Dukie,S., Li,Y. and Benson Wui-Man,L. (2022) RNA-binding protein signaling in adult neurogenesis. *Front Cell Dev Biol*, 10, 982549. doi: 10.3389/fcell.2022.982549.

5. Bryant,C.D. and Yazdani,N. (2016) RNA-binding proteins, neural development and the addictions. *Genes Brain Behav*, 15, 169–186. doi: 10.1111/gbb.12273.

6. Prashad,S. and Gopal,P.P. (2021) RNA-binding proteins in neurological development and disease. *RNA Biol*, 18, 972–987. doi: 10.1080/15476286.2020.1809186.

7. Marcelino Meliso,F., Hubert,C.G., Favoretto Galante,P.A. and Penalva,L.O. (2017) RNA processing as an alternative route to attack glioblastoma. *Hum Genet*, 136, 1129–1141. doi: 10.1007/s00439-017-1819-2.

8. Sanya,D.R.A., Cava,C. and Onésime,D. (2023) Roles of RNA-binding proteins in neurological disorders, COVID-19, and cancer. *Hum Cell*, 36, 493–514. doi: 10.1007/s13577-022-00843-w.

9. Kavanagh,T., Halder,A. and Drummond,E. (2022) Tau interactome and RNA binding proteins in neurodegenerative diseases. *Mol Neurodegener*, 17, 66. doi: 10.1186/s13024-022-00572-6.

10. Velasco MX, Kosti A, Penalva LOF and Hernández G (2019) The diverse roles of RNA-binding proteins in glioma development. *Adv Exp Med Biol*, 1157, 29–39.

11. Gebauer,F., Schwarzl,T., Valcárcel,J. and Hentze,M.W. (2021) RNA-binding proteins in human genetic disease. *Nat Rev Genet*, 22, 185–198. doi: 10.1038/s41576-020-00302-y.

12. Nussbacher,J.K., Batra,R., Lagier-Tourenne,C. and Yeo,G.W. (2015) RNA-binding proteins in neurodegeneration: seq and you shall receive. *Trends Neurosci*, 38, 226–236. doi: 10.1016/j.tins.2015.02.003.
13. An,H., de Meritens,C.R. and Shelkovnikova,T.A. (2021) Connecting the “dots”: RNP granule network in health and disease. *Biochim Biophys Acta Mol Cell Res*, 1868, 119058. doi: 10.1016/j.bbamcr.2021.119058.
14. Drino,A. and Schaefer,M.R. (2018) RNAs, phase separation, and membrane-less organelles: are post-transcriptional modifications modulating organelle dynamics? *Bioessays*, 40, e1800085. doi: 10.1002/bies.201800085.
15. Gomes,E. and Shorter,J. (2019) The molecular language of membraneless organelles. *J Biol Chem*, 294, 7115–7127. doi: 10.1074/jbc.TM118.001192.
16. Zeke,A., Schád,É., Horváth,T., Abukhairan,R., Szabó,B. and Tantos,A. (2022) Deep structural insights into RNA-binding disordered protein regions. *Wiley Interdiscip Rev RNA*, 13, e1714. doi: 10.1002/wrna.1714.
17. Roden,C. and Gladfelter,A.S. (2021) RNA contributions to the form and function of biomolecular condensates. *Nat Rev Mol Cell Biol*, 22, 183–195. doi: 10.1038/s41580-020-0264-6.
18. Cave,J.W. and Willis,D.E. (2022) 33905176 G-quadruplex regulation of neural gene expression. *FEBS J*, 289, 3284–3303. doi: 10.1111/febs.15900.
19. Masai,H. and Tanaka,T. (2020) G-quadruplex DNA and RNA: their roles in regulation of DNA replication and other biological functions. *Biochem Biophys Res Commun*, 531, 25–38. doi: 10.1016/j.bbrc.2020.05.132.
20. Nakanishi,C. and Seimiya,H. (2020) G-quadruplex in cancer biology and drug discovery. *Biochem Biophys Res Commun*, 531, 45–50. doi: 10.1016/j.bbrc.2020.03.178.
21. Kosiol,N., Juranek,S., Brossart,P., Heine,A. and Paeschke,K. (2021) G-quadruplexes: a promising target for cancer therapy. *Mol Cancer*, 20, 40. doi: 10.1186/s12943-021-01328-4.
22. Darling,A.L. and Shorter,J. (2021) Combating deleterious phase transitions in neurodegenerative disease. *Biochim Biophys Acta Mol Cell Res*, 1868, 118984. doi: 10.1016/j.bbamcr.2021.118984.
23. Webber,C.J., Lei,S. (Eric) and Wolozin,B. (2020) The pathophysiology of neurodegenerative disease: disturbing the balance between phase separation and irreversible aggregation. *Prog Mol Biol Transl Sci*, 174, 187–223. doi: 10.1016/bs.pmbts.2020.04.021.
24. Uversky,V.N. (2017) The roles of intrinsic disorder-based liquid-liquid phase transitions in the “Dr. Jekyll–Mr. Hyde” behavior of proteins involved in amyotrophic lateral sclerosis and frontotemporal lobar degeneration. *Autophagy*, 13, 2115–2162. doi: 10.1080/15548627.2017.1384889.
25. Baudin,A., Moreno-Romero,A.K., Xu,X., Selig,E.E., Penalva,L.O.F. and Libich,D.S. (2021) Structural characterization of the RNA-binding protein SERBP1 reveals intrinsic disorder and atypical RNA binding modes. *Front Mol Biosci*, 8, 744707. doi: 10.3389/fmolb.2021.744707.
26. Kosti,A., De Araujo,P.R., Li,W.Q., Guardia,G.D.A., Chiou,J., Yi,C., Ray,D., Meliso,F., Li,Y.M., Delambre,T., *et al.* (2020) The RNA-binding protein SERBP1 functions as a novel oncogenic factor in glioblastoma by bridging cancer metabolism and epigenetic regulation. *Genome Biol*, 21, 195. doi: 10.1186/s13059-020-02115-y.
27. Xijin Ge,S., Jung,D. and Yao,R. (2020) ShinyGO: a graphical gene-set enrichment tool for animals and plants. *Bioinformatics*, 36, 2628–2629. doi: 10.1093/bioinformatics/btz931.
28. Zhou,Y., Zhou,B., Pache,L., Chang,M., Khodabakhshi,A.H., Tanaseichuk,O., Benner,C. and Chanda,S.K. (2019) Metascape provides a biologist-oriented resource for the analysis of systems-level datasets. *Nat Commun*, 10, 1523. doi: 10.1038/s41467-019-09234-6.
29. Supek,F., Bošnjak,M., Škunca,N. and Šmuc,T. (2011) Revigo summarizes and visualizes long lists of gene ontology terms. *PLoS One*, 6, e21800. doi: 10.1371/journal.pone.0021800.

30. Go,C.D., Knight,J.D.R., Rajasekharan,A., Rathod,B., Hesketh,G.G., Abe,K.T., Youn,J.Y., Samavarchi-Tehrani,P., Zhang,H., Zhu,L.Y., *et al.* (2021) A proximity-dependent biotinylation map of a human cell. *Nature*, 595, 120–124. doi: 10.1038/s41586-021-03592-2.
31. Youn,J.Y., Dunham,W.H., Hong,S.J., Knight,J.D.R., Bashkurov,M., Chen,G.I., Bagci,H., Rathod,B., MacLeod,G., Eng,S.W.M., *et al.* (2018) High-density proximity mapping reveals the subcellular organization of mRNA-associated granules and bodies. *Mol Cell*, 69, 517-532.e11. doi: 10.1016/j.molcel.2017.12.020.
32. Stark,C., Breitkreutz,B.J., Reguly,T., Boucher,L., Breitkreutz,A. and Tyers,M. (2006) BioGRID: a general repository for interaction datasets. *Nucleic Acids Res*, 34, D535–D539. doi: 10.1093/nar/gkj109.
33. Brown,A., Baird,M.R., Cj Yip,M., Murray,J. and Shao,S. (2018) Structures of translationally inactive mammalian ribosomes. *Elife*, 7, e40486. doi: 10.7554/eLife.40486.
34. Muto,A., Sugihara,Y., Shibakawa,M., Oshima,K., Matsuda,T. and Nadano,D. (2018) The mRNA-binding protein Serbp1 as an auxiliary protein associated with mammalian cytoplasmic ribosomes. *Cell Biochem Funct*, 36, 312–322. doi: 10.1002/cbf.3350.
35. Ahn,J.W., Kim,S., Na,W., Baek,S.J., Kim,J.H., Min,K., Yeom,J., Kwak,H., Jeong,S., Lee,C., *et al.* (2015) SERBP1 affects homologous recombination-mediated DNA repair by regulation of CtIP translation during S phase. *Nucleic Acids Res*, 43, 6321–6333. doi: 10.1093/nar/gkv592.
36. Martini,S., Davis,K., Faraway,R., Elze,L., Lockwood,N., Jones,A., Xie,X., McDonald,N.Q., Mann,D.J., Armstrong,A., *et al.* (2021) A genetically-encoded crosslinker screen identifies SERBP1 as a PKCε substrate influencing translation and cell division. *Nat Commun*, 12, 6934. doi: 10.1038/s41467-021-27189-5.
37. Lee,Y., Jen, Wei,H.M., Chen,L.Y. and Li,C. (2014) Localization of SERBP1 in stress granules and nucleoli. *FEBS J*, 281, 352–364. doi: 10.1111/febs.12606.
38. Lee,Y.J., Hsieh,W.Y., Chen,L.Y. and Li,C. (2012) Protein arginine methylation of SERBP1 by protein arginine methyltransferase 1 affects cytoplasmic/nuclear distribution. *J Cell Biochem*, 113, 2721–2728. doi: 10.1002/jcb.24151.
39. Passos,D.O., Bressan,G.C., Nery,F.C. and Kobarg,J. (2006) Ki-1/57 interacts with PRMT1 and is a substrate for arginine methylation. *FEBS J*, 273, 3946–3961. doi: 10.1111/j.1742-4658.2006.05399.x.
40. Coppolecchia,R., Buser,P., Stotz,A. and Linder,P. (1993) A new yeast translation initiation factor suppresses a mutation in the elF-4A RNA helicase. *EMBO J*, 12, 4005–4011.
41. Bleckmann,A., Spitzlberger,N., Denninger,P., Ehrnsberger,H.F., Wang,L., Bruckmann,A., Reich,S., Holzinger,P., Medenbach,J., Grasser,K.D., *et al.* (2023) Cytosolic RGG RNA-binding proteins are temperature sensitive flowering time regulators in Arabidopsis. *Biol Chem*, 404, 1069–1084. doi: 10.1515/hsz-2023-0171.
42. Sonnhammer,E.L., Eddy,S.R. and Durbin,R. (1997) Pfam: a comprehensive database of protein domain families based on seed alignments. *Proteins*, 28, 405–420. doi: 10.1002/(SICI)1097-0134(199707)28:3<405::AID-PROT10>3.0.CO;2-L.
43. Fonin,A. V., Antifeeva,I.A., Kuznetsova,I.M., Turoverov,K.K., Zaslavsky,B.Y., Kulkarni,P. and Uversky,V.N. (2022) Biological soft matter: intrinsically disordered proteins in liquid-liquid phase separation and biomolecular condensates. *Essays Biochem*, 66, 831–847. doi: 10.1042/EBC20220052.
44. Su,Q., Mehta,S. and Zhang,J. (2021) Liquid-liquid phase separation: orchestrating cell signaling through time and space. *Mol Cell*, 81, 4137–4146. doi: 10.1016/j.molcel.2021.09.010.
45. Piovesan,D., Del Conte,A., Clementel,D., Monzon,A.M., Bevilacqua,M., Aspromonte,M.C., Iserte,J.A., Orti,F.E., Marino-Buslje,C. and Tosatto,S.C.E. (2023) MobiDB: 10 years of intrinsically disordered proteins. *Nucleic Acids Res*, 51, D438–D444. doi: 10.1093/nar/gkac1065.
46. Su,H., Xu,J., Chen,Y., Wang,Q., Lu,Z., Chen,Y., Chen,K., Han,S., Fang,Z., Wang,P., *et al.* (2021) Photoactive G-quadruplex ligand identifies multiple G-quadruplex-related proteins with

extensive sequence tolerance in the cellular environment. *J Am Chem Soc*, 143, 1917–1923. doi: 10.1021/jacs.0c10792.
47. Herviou,P., Le Bras,M., Dumas,L., Hieblot,C., Gilhodes,J., Cioci,G., Hugnot,J.P., Ameadan,A., Guillonneau,F., Dassi,E., *et al.* (2020) hnRNP H/F drive RNA G-quadruplex-mediated translation linked to genomic instability and therapy resistance in glioblastoma. *Nat Commun*, 11, 2661. doi: 10.1038/s41467-020-16168-x.
48. Huang,Z.L., Dai,J., Luo,W.H., Wang,X.G., Tan,J.H., Chen,S. Bin and Huang,Z.S. (2018) Identification of G-quadruplex-binding protein from the exploration of RGG motif/G-quadruplex interactions. *J Am Chem Soc*, 140, 17945–17955. doi: 10.1021/jacs.8b09329.
49. Patra,S., Claude,J.B., Naubron,J.V. and Wenger,J. (2021) Fast interaction dynamics of G-quadruplex and RGG-rich peptides unveiled in zero-mode waveguides. *Nucleic Acids Res*, 49, 12348–12357. doi: 10.1093/nar/gkab1002.
50. Thandapani,P., O'Connor,T.R., Bailey,T.L. and Richard,S. (2013) Defining the RGG/RG Motif. *Mol Cell*, 50, 613–623. doi: 10.1016/j.molcel.2013.05.021.
51. Herdy,B., Mayer,C., Varshney,D., Marsico,G., Murat,P., Taylor,C., D'Santos,C., Tannahill,D. and Balasubramanian,S. (2018) Analysis of NRAS RNA G-quadruplex binding proteins reveals DDX3X as a novel interactor of cellular G-quadruplex containing transcripts. *Nucleic Acids Res*, 46, 11592–11604. doi: 10.1093/nar/gky861.
52. McRae,E.K.S., Dupas,S.J., Booy,E.P., Piragasam,R.S., Fahlman,R.P. and McKenna,S.A. (2020) An RNA guanine quadruplex regulated pathway to TRAIL-sensitization by DDX21. *RNA*, 26, 44–57. doi: 10.1261/rna.072199.119.
53. Murat,P., Marsico,G., Herdy,B., Ghanbarian,A.T., Portella,G. and Balasubramanian,S. (2018) RNA G-quadruplexes at upstream open reading frames cause DHX36- and DHX9-dependent translation of human mRNAs. *Genome Biol*, 19, 229. doi: 10.1186/s13059-018-1602-2.
54. Varshney,D., Cuesta,S.M., Herdy,B., Abdullah,U.B., Tannahill,D. and Balasubramanian,S. (2021) RNA G-quadruplex structures control ribosomal protein production. *Sci Rep*, 11, 22735. doi: 10.1038/s41598-021-01847-6.
55. Ruggiero,E. and Richter,S.N. (2018) G-quadruplexes and G-quadruplex ligands: Targets and tools in antiviral therapy. *Nucleic Acids Res*, 46, 3270–3283. doi: 10.1093/nar/gky187.
56. Xu,J., Huang,H. and Zhou,X. (2021) G-Quadruplexes in neurobiology and virology: functional roles and potential therapeutic approaches. *JACS Au*, 1, 2146–2161. doi: 10.1021/jacsau.1c00451.
57. Lee,S., Lee,Y.S., Choi,Y., Son,A., Park,Y., Lee,K.M., Kim,J., Kim,J.S. and Kim,V.N. (2021) The SARS-CoV-2 RNA interactome. *Mol Cell*, 81, 2838-2850.e6. doi: 10.1016/j.molcel.2021.04.022.
58. Chung,K.S., Won,M., Lee,J.J., Ahn,J., Hoe,K.L., Kim,D.U., Song,K. Bin and Yoo,H.S. (2007) 17346842 Yeast-based screening to identify modulators of G-protein signaling using uncontrolled cell division cycle by overexpression of Stm1. *J Biotechnol*, 129, 547–554. doi: 10.1016/j.jbiotec.2007.01.007.
59. Kim,D.S., Challa,S., Jones,A. and Kraus,W.L. (2020) PARPs and ADP-ribosylation in RNA biology: from RNA expression and processing to protein translation and proteostasis. *Genes Dev*, 34, 302–320. doi: 10.1101/gad.334433.119.
60. Gupte,R., Liu,Z. and Kraus,W.L. (2017) PARPs and ADP-ribosylation: recent advances linking molecular functions to biological outcomes. *Genes Dev*, 31, 101–126. doi: 10.1101/gad.291518.
61. Huang,D. and Kraus,W.L. (2022) The expanding universe of PARP1-mediated molecular and therapeutic mechanisms. *Mol Cell*, 82, 2315–2334. doi: 10.1016/j.molcel.2022.02.021.
62. Gibson,B.A., Zhang,Y., Jiang,H., Hussey,K.M., Shrimp,J.H., Lin,H., Schwede,F., Yu,Y. and Kraus,W.L. (2016) Chemical genetic discovery of PARP targets reveals a role for PARP-1 in transcription elongation. *Science*, 353, 45–50. doi: 10.1126/science.aaf7865.

63. Martello,R., Leutert,M., Jungmichel,S., Bilan,V., Larsen,S.C., Young,C., Hottiger,M.O. and Nielsen,M.L. (2016) Proteome-wide identification of the endogenous ADP-ribosylome of mammalian cells and tissue. *Nat Commun*, 7, 12917. doi: 10.1038/ncomms12917.
64. Dasovich,M., Beckett,M.Q., Bailey,S., Ong,S.E., Greenberg,M.M. and Leung,A.K.L. (2021) Identifying poly(ADP-ribose)-binding proteins with photoaffinity-based proteomics. *J Am Chem Soc*, 143, 3037–3042. doi: 10.1021/jacs.0c12246.
65. Zhang,C., Guo,Q., Chen,L., Wu,Z., Yan,X.J., Zou,C., Zhang,Q., Tan,J., Fang,T., Rao,Q., *et al.* (2023) A ribosomal gene panel predicting a novel synthetic lethality in non-BRCAness tumors. *Signal Transduct Target Ther*, 8, 183. doi: 10.1038/s41392-023-01401-y.
66. Mosler,T., Baymaz,H.I., Gräf,J.F., Mikicic,I., Blattner,G., Bartlett,E., Ostermaier,M., Piccinno,R., Yang,J., Voigt,A., *et al.* (2022) PARP1 proximity proteomics reveals interaction partners at stressed replication forks. *Nucleic Acids Res*, 50, 11600–11618. doi: 10.1093/nar/gkac948.
67. Kim,D.S., Camacho,C. V., Nagari,A., Malladi,V.S., Challa,S. and Kraus,W.L. (2019) Activation of PARP-1 by snoRNAs controls ribosome biogenesis and cell growth via the RNA helicase DDX21. *Mol Cell*, 75, 1270-1285.e14. doi: 10.1016/j.molcel.2019.06.020.
68. Mekishvili,M., Matveeva,E. and Fondufe-Mittendorf,Y. (2017) Methodology to identify poly-ADP-ribose polymerase 1 (PARP1)-mRNA targets by PAR-CLiP. *Methods Mol Biol,* 1608, 211–228. doi: 10.1007/978-1-4939-6993-7_15.
69. Wei,H. and Yu,X. (2016) Functions of PARylation in DNA damage repair pathways. *Genomics Proteomics Bioinformatics*, 14, 131–139. doi: 10.1016/j.gpb.2016.05.001.
70. Žaja,R., Mikoč,A., Barkauskaite,E. and Ahel,I. (2012) Molecular insights into poly(ADP-ribose) recognition and processing. *Biomolecules*, 3, 1–17. doi: 10.3390/biom3010001.
71. UniProt Consortium (2023) UniProt: The universal protein knowledgebase in 2023. *Nucleic Acids Res*, 51, D523–D531. doi: 10.1093/nar/gkac1052.
72. Thomas,P.D., Ebert,D., Muruganujan,A., Mushayahama,T., Albou,L.P. and Mi,H. (2022) PANTHER: Making genome-scale phylogenetics accessible to all. *Protein Sci*, 31, 8–22. doi: 10.1002/pro.4218.
73. Li,W., Jiang,C. and Zhang,E. (2021) Advances in the phase separation-organized membraneless organelles in cells: a narrative review. *Transl Cancer Res*, 10, 4929–4946. doi: 10.21037/tcr-21-1111.
74. Kastano,K., Mier,P., Dosztányi,Z., Promponas,V.J. and Andrade-Navarro,M.A. (2022) Functional tuning of intrinsically disordered regions in human proteins by composition bias. *Biomolecules*, 12, 1486. doi: 10.3390/biom12101486.
75. Feng,Z., Jia,B. and Zhang,M. (2021) Liquid-liquid phase separation in biology: specific stoichiometric molecular interactions vs promiscuous interactions mediated by disordered sequences. *Biochemistry*, 60, 2397–2406. doi: 10.1021/acs.biochem.1c00376.
76. Kimura,T., Sharma,G., Ishiguro,K. and Hisanaga,S.I. (2018) Phospho-Tau bar code: analysis of phosphoisotypes of Tau and its application to tauopathy. *Front Neurosci*, 12, 44. doi: 10.3389/fnins.2018.00044.
77. Lester,E., Ooi,F.K., Bakkar,N., Ayers,J., Woerman,A.L., Wheeler,J., Bowser,R., Carlson,G.A., Prusiner,S.B. and Parker,R. (2021) Tau aggregates are RNA-protein assemblies that mislocalize multiple nuclear speckle components. *Neuron*, 109, 1675-1691.e9. doi: 10.1016/j.neuron.2021.03.026.
78. Hernández-Ortega,K., Garcia-Esparcia,P., Gil,L., Lucas,J.J. and Ferrer,I. (2016) Altered machinery of protein synthesis in Alzheimer's: from the nucleolus to the ribosome. *Brain Pathol*, 26, 593–605. doi: 10.1111/bpa.12335.
79. Evans,H.T., Taylor,D., Kneynsberg,A., Bodea,L.G. and Götz,J. (2021) Altered ribosomal function and protein synthesis caused by tau. *Acta Neuropathol Commun*, 9, 110. doi: 10.1186/s40478-021-01208-4.

80. Mao,K. and Zhang,G. (2022) The role of PARP1 in neurodegenerative diseases and aging. *FEBS J*, 289, 2013–2024. doi: 10.1111/febs.15716.
81. Ash,P.E.A., Vanderweyde,T.E., Youmans,K.L., Apicco,D.J. and Wolozin,B. (2014) Pathological stress granules in Alzheimer's disease. *Brain Res*, 1584, 52–58. doi: 10.1016/j.brainres.2014.05.052.
82. Vanderweyde,T., Yu,H., Varnum,M., Liu-Yesucevitz,L., Citro,A., Ikezu,T., Duff,K. and Wolozin,B. (2012) Contrasting pathology of the stress granule proteins TIA-1 and G3BP in tauopathies. *J Neurosci*, 32, 8270–8283. doi: 10.1523/JNEUROSCI.1592-12.2012.
83. Heaton,J.H., Dlakic,W.M., Dlakic,M. and Gelehrter,T.D. (2001) Identification and cDNA cloning of a novel RNA-binding protein that interacts with the cyclic nucleotide-responsive sequence in the Type-1 plasminogen activator Inhibitor mRNA. *J Biol Chem*, 276, 3341–3347. doi: 10.1074/jbc.M006538200.
84. Van Dyke,N., Baby,J. and Van Dyke,M.W. (2006) Stm1p, a ribosome-associated protein, is important for protein synthesis in Saccharomyces cerevisiae under nutritional stress conditions. *J Mol Biol*, 358, 1023–1031. doi: 10.1016/j.jmb.2006.03.018.
85. Mateju,D., Eichenberger,B., Voigt,F., Eglinger,J., Roth,G. and Chao,J.A. (2020) Single-molecule imaging reveals translation of mRNAs localized to stress granules. *Cell*, 183, 1801-1812.e13. doi: 10.1016/j.cell.2020.11.010.
86. Ray,S. and Anderson,E.C. (2016) Stimulation of translation by human Unr requires cold shock domains 2 and 4, and correlates with poly(A) binding protein interaction. *Sci Rep*, 6, 22461. doi: 10.1038/srep22461.
87. Mitchell,S.A., Brown,E.C., Coldwell,M.J., Jackson,R.J. and Willis,A.E. (2001) Protein factor requirements of the Apaf-1 internal ribosome entry segment: Roles of polypyrimidine tract binding protein and upstream of N-ras. *Mol Cell Biol*, 21, 3364–3374. doi: 10.1128/mcb.21.10.3364-3374.2001.
88. Dormoy-Raclet,V., Markovits,J., Jacquemin-Sablon,A. and Jacquemin-Sablon,H. (2005) Regulation of Unr expression by 5′- and 3′-untranslated regions of its mRNA through modulation of stability and IRES mediated translation. *RNA Biol*, 2, e27-35. doi: 10.4161/rna.2.3.2203.
89. Abaza,I., Coll,O., Patalano,S. and Gebauer,F. (2006) Drosophila UNR is required for translational repression of male-specific lethal 2 mRNA during regulation of X-chromosome dosage compensation. *Genes Dev*, 20, 380–389. doi: 10.1101/gad.371906.
90. Guo,A.X., Cui,J.J., Wang,L.Y. and Yin,J.Y. (2020) The role of CSDE1 in translational reprogramming and human diseases. *Cell Commun Signal*, 18, 14. doi: 10.1186/s12964-019-0496-2.
91. Walsh,D. and Mohr,I. (2011) Viral subversion of the host protein synthesis machinery. *Nat Rev Microbiol*, 9, 860–875. doi: 10.1038/nrmicro2655.
92. Locker,N., Chamond,N. and Sargueil,B. (2011) A conserved structure within the HIV gag open reading frame that controls translation initiation directly recruits the 40S subunit and eIF3. *Nucleic Acids Res*, 39, 2367–2377. doi: 10.1093/nar/gkq1118.
93. Boussadia,O., Niepmann,M., Créancier,L., Prats,A.C., Dautry,F. and Jacquemin-Sablon,H. (2003) Unr is required in vivo for efficient initiation of translation from the internal ribosome entry sites of both rhinovirus and poliovirus. *J Virol*, 77, 3353–3359. doi: 10.1128/jvi.77.6.3353-3359.2003.
94. Brugier,A., Hafirrassou,M.L., Pourcelot,M., Baldaccini,M., Kril,V., Couture,L., Kümmerer,B.M., Gallois-Montbrun,S., Bonnet-Madin,L., Vidalain,P.O., *et al.* (2022) RACK1 associates with RNA-binding proteins Vigilin and SERBP1 to facilitate dengue virus replication. *J Virol*, 96, e0196221. doi: 10.1128/jvi.01962-21.
95. Tollervey,D. and Kiss,T. (1997) Function and synthesis of small nucleolar RNAs. *Curr Opin Cell Biol*, 9, 337–342. doi: 10.1016/s0955-0674(97)80005-1.
96. Tafforeau,L., Zorbas,C., Langhendries,J.L., Mullineux,S.T., Stamatopoulou,V., Mullier,R., Wacheul,L. and Lafontaine,D.L.J. (2013) The complexity of human ribosome biogenesis

revealed by systematic nucleolar screening of pre-rRNA processing factors. *Mol Cell*, 51, 539–551. doi: 10.1016/j.molcel.2013.08.011.
97. Tollervey,D., Lehtonen,H., Jansen,R., Kern,H. and Hurt,E.C. (1993) Temperature-sensitive mutations demonstrate roles for yeast fibrillarin in pre-rRNA processing, pre-rRNA methylation, and ribosome assembly. *Cell*, 72, 443–457. doi: 10.1016/0092-8674(93)90120-F.
98. Iyer-Bierhoff,A., Krogh,N., Tessarz,P., Ruppert,T., Nielsen,H. and Grummt,I. (2018) SIRT7-dependent deacetylation of Fibrillarin controls Histone H2A methylation and rRNA synthesis during the cell cycle. *Cell Rep*, 25, 2946-2954.e5. doi: 10.1016/j.celrep.2018.11.051.
99. Herdman,C., Mars,J.C., Stefanovsky,V.Y., Tremblay,M.G., Sabourin-Felix,M., Lindsay,H., Robinson,M.D. and Moss,T. (2017) A unique enhancer boundary complex on the mouse ribosomal RNA genes persists after loss of Rrn3 or UBF and the inactivation of RNA polymerase I transcription. *PLoS Genet*, 13, e1006899. doi: 10.1371/journal.pgen.1006899.
100. Bose,T., Lee,K.K., Lu,S., Xu,B., Harris,B., Slaughter,B., Unruh,J., Garrett,A., McDowell,W., Box,A., *et al.* (2012) Cohesin proteins promote ribosomal RNA production and protein translation in yeast and human cells. *PLoS Genet*, 8, e1002749. doi: 10.1371/journal.pgen.1002749.
101. Calo,E., Flynn,R.A., Martin,L., Spitale,R.C., Chang,H.Y. and Wysocka,J. (2015) 25470060 RNA helicase DDX21 coordinates transcription and ribosomal RNA processing. *Nature*, 518, 249–253. doi: 10.1038/nature13923.
102. Ugrinova,I., Petrova,M., Chalabi-Dchar,M. and Bouvet,P. (2018) Multifaceted Nucleolin protein and its molecular partners in oncogenesis. *Adv Protein Chem Struct Biol*, 111, 133–164. doi: 10.1016/bs.apcsb.2017.08.001.
103. Hendriks,I.A., Larsen,S.C. and Nielsen,M.L. (2019) An advanced strategy for comprehensive profiling of ADP-ribosylation sites using mass spectrometry-based proteomics. *Molecular Cell Proteomics*, 18, 1010–1026. doi: 10.1074/mcp.TIR119.001315.
104. Bonfiglio,J.J., Fontana,P., Zhang,Q., Colby,T., Gibbs-Seymour,I., Atanassov,I., Bartlett,E., Zaja,R., Ahel,I. and Matic,I. (2017) Serine ADP-ribosylation depends on HPF1. *Mol Cell*, 65, 932-940.e6. doi: 10.1016/j.molcel.2017.01.003.
105. Bilan,V., Selevsek,N., Kistemaker,H.A. V., Abplanalp,J., Feurer,R., Filippov,D. V. and Hottiger,M.O. (2017) New quantitative mass spectrometry approaches reveal different ADP-ribosylation phases dependent on the levels of oxidative stress. *Molecular Cell Proteomics*, 16, 949–958. doi: 10.1074/mcp.O116.065623.
106. Larsen,S.C., Hendriks,I.A., Lyon,D., Jensen,L.J. and Nielsen,M.L. (2018) Systems-wide analysis of Serine ADP-ribosylation reveals widespread occurrence and site-specific overlap with phosphorylation. *Cell Rep*, 24, 2493-2505.e4. doi: 10.1016/j.celrep.2018.07.083.
107. Tao,Z., Gao,P. and Liu,H.W. (2009) Studies of the expression of human poly(ADP-ribose) polymerase-1 in Saccharomyces cerevisiae and identification of PARP-1 substrates by yeast proteome microarray screening. *Biochemistry*, 48, 11745–11754. doi: 10.1021/bi901387k.
108. Manco,G., Lacerra,G., Porzio,E. and Catara,G. (2022) ADP-ribosylation post-translational modification: an overview with a focus on RNA biology and new pharmacological perspectives. *Biomolecules*, 12, 443. doi: 10.3390/biom12030443.
109. Duan,Y., Du,A., Gu,J., Duan,G., Wang,C., Gui,X., Ma,Z., Qian,B., Deng,X., Zhang,K., *et al.* (2019) PARylation regulates stress granule dynamics, phase separation, and neurotoxicity of disease-related RNA-binding proteins. *Cell Res*, 29, 233–247. doi: 10.1038/s41422-019-0141-z.
110. Melikishvili,M., Chariker,J.H., Rouchka,E.C. and Fondufe-Mittendorf,Y.N. (2017) Transcriptome-wide identification of the RNA-binding landscape of the chromatin-associated protein PARP1 reveals functions in RNA biogenesis. *Cell Discov*, 3, 17043. doi: 10.1038/celldisc.2017.43.
111. Leung,A.K.L. (2020) Poly(ADP-ribose): a dynamic trigger for biomolecular condensate formation. *Trends Cell Biol*, 30, 370–383. doi: 10.1016/j.tcb.2020.02.002.

112. Ottoz,D.S.M. and Berchowitz,L.E. (2020) The role of disorder in RNA binding affinity and specificity: the role of disorder in RNA binding. *Open Biol*, 10, 200328. doi: 10.1098/rsob.200328.
113. Naskar,A., Nayak,A., Salaikumaran,M.R., Vishal,S.S. and Gopal,P.P. (2023) Phase separation and pathologic transitions of RNP condensates in neurons: implications for amyotrophic lateral sclerosis, frontotemporal dementia and other neurodegenerative disorders. *Front Mol Neurosci*, 16, 1242925. doi: 10.3389/fnmol.2023.1242925.
114. Lyu,K., Chow,E.Y.C., Mou,X., Chan,T.F. and Kwok,C.K. (2021) RNA G-quadruplexes (rG4s): genomics and biological functions. *Nucleic Acids Res*, 49, 5426–5450. doi: 10.1093/nar/gkab187.
115. Banco,M.T. and Ferré-D'Amaré,A.R. (2021) The emerging structural complexity of G-quadruplex RNAs. *RNA*, 27, 390–402. doi: 10.1261/rna.078238.120.
116. Dumas,L., Herviou,P., Dassi,E., Cammas,A. and Millevoi,S. (2021) G-quadruplexes in RNA biology: recent advances and future directions. *Trends Biochem Sci*, 46, 270–283. doi: 10.1016/j.tibs.2020.11.001.
117. Edwards,A.D., Marecki,J.C., Byrd,A.K., Gao,J. and Raney,K.D. (2021) G-quadruplex loops regulate PARP-1 enzymatic activation. *Nucleic Acids Res*, 49, 416–431. doi: 10.1093/nar/gkaa1172.
118. Bleuzé,L., Triaca,V. and Borreca,A. (2021) FMRP-driven neuropathology in Autistic spectrum disorder and Alzheimer's disease: A losing game. *Front Mol Biosci*, 8, 699613. doi: 10.3389/fmolb.2021.699613.
119. Fyke,W. and Velinov,M. (2021) Fmr1 and autism, an intriguing connection revisited. *Genes (Basel)*, 12, 1218. doi: 10.3390/genes12081218.
120. Davis,J.K. and Broadie,K. (2017) Multifarious functions of the Fragile X mental retardation protein. *Trends Genet,* 33, 703–714. doi: 10.1016/j.tig.2017.07.008.
121. Darnell,J.C., Warren,S.T. and Darnell,R.B. (2004) The Fragile X mental retardation protein, FMRP, recognizes G-quartets. *Ment Retard Dev Disabil Res Rev*, 10, 49–52. doi: 10.1002/mrdd.20008.
122. Darnell,J.C. and Klann,E. (2013) The translation of translational control by FMRP: therapeutic targets for FXS. *Nat Neurosci*, 16, 1530–1536. doi: 10.1038/nn.3379.
123. Richter,J.D. and Zhao,X. (2021) The molecular biology of FMRP: new insights into fragile X syndrome. *Nat Rev Neurosci*, 22, 209–222. doi: 10.1038/s41583-021-00432-0.
124. Chen,H.H., Yu,H.I., Chiang,W.C., Lin,Y. De, Shia,B.C. and Tarn,W.Y. (2012) hnRNP Q regulates Cdc42-mediated neuronal morphogenesis. *Mol Cell Biol*, 32, 2224–2238. doi: 10.1128/mcb.06550-11.
125. Duning,K., Buck,F., Barnekow,A. and Kremerskothen,J. (2008) SYNCRIP, a component of dendritically localized mRNPs, binds to the translation regulator BC200 RNA. *J Neurochem*, 105, 351–359. doi: 10.1111/j.1471-4159.2007.05138.x.
126. Khudayberdiev,S., Soutschek,M., Ammann,I., Heinze,A., Rust,M.B., Baumeister,S. and Schratt,G. (2021) The cytoplasmic SYNCRIP mRNA interactome of mammalian neurons. *RNA Biol*, 18, 1252–1264. doi: 10.1080/15476286.2020.1830553.
127. Titlow,J., Robertson,F., Järvelin,A., Ish-Horowicz,D., Smith,C., Gratton,E. and Davis,I. (2020) Syncrip/hnRNP Q is required for activity-induced Msp300/Nesprin-1 expression and new synapse formation. *J Cell Biol*, 219, e201903135. doi: 10.1083/jcb.201903135.
128. Halstead,J.M., Lin,Y.Q., Durraine,L., Hamilton,R.S., Ball,G., Neely,G.G., Bellen,H.J. and Davis,I. (2014) Syncrip/hnRNP Q influences synaptic transmission and regulates BMP signaling at the Drosophila neuromuscular synapse. *Biol Open*, 3, 839–849. doi: 10.1242/bio.20149027.
129. Sapir,T., Kshirsagar,A., Gorelik,A., Olender,T., Porat,Z., Scheffer,I.E., Goldstein,D.B., Devinsky,O. and Reiner,O. (2022) Heterogeneous nuclear ribonucleoprotein U (HNRNPU) safeguards the developing mouse cortex. *Nat Commun*, 13, 4209. doi: 10.1038/s41467-022-31752-z.

130. Lelieveld,S.H., Reijnders,M.R.F., Pfundt,R., Yntema,H.G., Kamsteeg,E.J., De Vries,P., De Vries,B.B.A., Willemsen,M.H., Kleefstra,T., Löhner,K., *et al.* (2016) Meta-analysis of 2,104 trios provides support for 10 new genes for intellectual disability. *Nat Neurosci*, 19, 1194–1196. doi: 10.1038/nn.4352.
131. Balasubramanian,M. (2022) HNRNPU-related neurodevelopmental disorder. In Adam,M.P., Mirzaa,G.M., Pagon,R.A., Wallace,S.E., Bean,L.J.H., Gripp,K.W., Amemiya,A. (eds), *GeneReviews® [Internet]*. Seattle (WA): University of Washington, Seattle, pp. 1993–2023.
132. Bramswig,N.C., Lüdecke,H.J., Hamdan,F.F., Altmüller,J., Beleggia,F., Elcioglu,N.H., Freyer,C., Gerkes,E.H., Demirkol,Y.K., Knupp,K.G., *et al.* (2017) Heterozygous HNRNPU variants cause early onset epilepsy and severe intellectual disability. *Hum Genet*, 136, 821–834. doi: 10.1007/s00439-017-1795-6.
133. Gillentine,M.A., Wang,T., Hoekzema,K., Rosenfeld,J., Liu,P., Guo,H., Kim,C.N., De Vries,B.B.A., Vissers,L.E.L.M., Nordenskjold,M., *et al.* (2021) Rare deleterious mutations of HNRNP genes result in shared neurodevelopmental disorders. *Genome Med*, 13, 63. doi: 10.1186/s13073-021-00870-6.
134. Wang,T., Hoekzema,K., Vecchio,D., Wu,H., Sulovari,A., Coe,B.P., Gillentine,M.A., Wilfert,A.B., Perez-Jurado,L.A., Kvarnung,M., *et al.* (2020) Large-scale targeted sequencing identifies risk genes for neurodevelopmental disorders. *Nat Commun*, 11, 4932. doi: 10.1038/s41467-020-18723-y.
135. Bakkar,N., Kovalik,T., Lorenzini,I., Spangler,S., Lacoste,A., Sponaugle,K., Ferrante,P., Argentinis,E., Sattler,R. and Bowser,R. (2018) Artificial intelligence in neurodegenerative disease research: use of IBM Watson to identify additional RNA-binding proteins altered in amyotrophic lateral sclerosis. *Acta Neuropathol*, 135, 227–247. doi: 10.1007/s00401-017-1785-8.
136. Keefe,A.D., Wilson,D.S., Seelig,B. and Szostak,J.W. (2001) One-step purification of recombinant proteins using a nanomolar-affinity streptavidin-binding peptide, the SBP-tag. *Protein Expr Purif*, 23, 440–446. doi: 10.1006/prep.2001.1515.
137. Huang,D., Camacho,C. V., Setlem,R., Ryu,K.W., Parameswaran,B., Gupta,R.K. and Kraus,W.L. (2020) Functional interplay between histone H2B ADP-ribosylation and phosphorylation controls adipogenesis. *Mol Cell*, 79, 934-949.e14. doi: 10.1016/j.molcel.2020.08.002.
138. Chou,T.C. (2010) Drug combination studies and their synergy quantification using the chou-talalay method. *Cancer Res*, 70, 440–446. doi: 10.1158/0008-5472.CAN-09-1947.
139. Szklarczyk,D., Kirsch,R., Koutrouli,M., Nastou,K., Mehryary,F., Hachilif,R., Gable,A.L., Fang,T., Doncheva,N.T., Pyysalo,S., *et al.* (2023) The STRING database in 2023: protein–protein association networks and functional enrichment analyses for any sequenced genome of interest. *Nucleic Acids Res*, 51, D638–D646. doi: 10.1093/nar/gkac1000.
140. Doncheva,N.T., Morris,J.H., Holze,H., Kirsch,R., Nastou,K.C., Cuesta-Astroz,Y., Rattei,T., Szklarczyk,D., von Mering,C. and Jensen,L.J. (2023) Cytoscape stringApp 2.0: analysis and visualization of heterogeneous biological networks. *J Proteome Res*, 22, 637–646. doi: 10.1021/acs.jproteome.2c00651.
141. Puchalski,R.B., Shah,N., Miller,J., Dalley,R., Nomura,S.R., Yoon,J.G., Smith,K.A., Lankerovich,M., Bertagnolli,D., Bickley,K., *et al.* (2018) An anatomic transcriptional atlas of human glioblastoma. *Science*, 360, 660–663. doi: 10.1126/science.aaf2666.
142. van de Leemput,J., Boles,N.C., Kiehl,T.R., Corneo,B., Lederman,P., Menon,V., Lee,C., Martinez,R.A., Levi,B.P., Thompson,C.L., *et al.* (2014) CORTECON: a temporal transcriptome analysis of in vitro human cerebral cortex development from human embryonic stem cells. *Neuron*, 83, 51–68. doi: 10.1016/j.neuron.2014.05.013.
143. Fang,H. and Gough,J. (2013) DcGO: database of domain-centric ontologies on functions, phenotypes, diseases and more. *Nucleic Acids Res*, 41, D536-544. doi: 10.1093/nar/gks1080.

144. Sutphin,G.L., Mahoney,J.M., Sheppard,K., Walton,D.O. and Korstanje,R. (2016) WORMHOLE: novel least diverged ortholog prediction through machine learning. *PLoS Comput Biol*, 12, e1005182. doi: 10.1371/journal.pcbi.1005182.
145. Kitts,P.A., Church,D.M., Thibaud-Nissen,F., Choi,J., Hem,V., Sapojnikov,V., Smith,R.G., Tatusova,T., Xiang,C., Zherikov,A., *et al.* (2016) Assembly: a resource for assembled genomes at NCBI. *Nucleic Acids Res*, 44, D73–D80. doi: 10.1093/nar/gkv1226.
146. Frankish,A., Diekhans,M., Jungreis,I., Lagarde,J., Loveland,J.E., Mudge,J.M., Sisu,C., Wright,J.C., Armstrong,J., Barnes,I., *et al.* (2021) GENCODE 2021. *Nucleic Acids Res*, 49, D916–D923. doi: 10.1093/nar/gkaa1087.
147. Dobin,A., Davis,C.A., Schlesinger,F., Drenkow,J., Zaleski,C., Jha,S., Batut,P., Chaisson,M. and Gingeras,T.R. (2013) STAR: ultrafast universal RNA-seq aligner. *Bioinformatics*, 29, 15–21. doi: 10.1093/bioinformatics/bts635.
148. Shen,S., Park,J.W., Lu,Z.X., Lin,L., Henry,M.D., Wu,Y.N., Zhou,Q. and Xing,Y. (2014) rMATS: robust and flexible detection of differential alternative splicing from replicate RNA-Seq data. *Proc Natl Acad Sci U S A*, 111, E5593–E5601. doi: 10.1073/pnas.1419161111.
149. Quinlan,A.R. and Hall,I.M. (2010) BEDTools: a flexible suite of utilities for comparing genomic features. *Bioinformatics*, 26, 841–842. doi: 10.1093/bioinformatics/btq033.
150. Bray,N.L., Pimentel,H., Melsted,P. and Pachter,L. (2016) Near-optimal probabilistic RNA-seq quantification. *Nat Biotechnol*, 34, 525–527. doi: 10.1038/nbt.3519.
151. Soneson,C., Love,M.I. and Robinson,M.D. (2015) Differential analyses for RNA-seq: transcript-level estimates improve gene-level inferences. *F1000Res*, 4, 1521. doi: 10.12688/f1000research.7563.1.
152. Love,M.I., Huber,W. and Anders,S. (2014) Moderated estimation of fold change and dispersion for RNA-seq data with DESeq2. *Genome Biol*, 15, 550. doi: 10.1186/s13059-014-0550-8.

Brain tissues analyzed in this study from diseased and age-matched non-demented control subjects are summarized.

Clinical Diagnosis	Case Number	Age	Gender	PMI (Hours)	Braak Tangles (0-6)	Application
AD	1154	86	M	3.25	6	IF/PLA
AD	1098	81	F	2.75	5	IF/PLA
AD	5773	74	M	10	5	IF/PLA
AD	5779	73	M	15	6	WB
AD	5781	88	M	10	5	WB
AD	5829	68	M	12	6	WB
Control	5263	88	M	12.17	1	IF/PLA
Control	1161	84	F	2.50	0	IF/PLA
Control	1106	79	M	1.75	2	IF/PLA
Control	1796	81	M	8	0	WB
Control	2-99	74	F	2.8	2	WB
Control	13-01	95	M	3.7	1	WB

IF: Immunofluorescence
PLA: Proximity Ligation Assay
PMI: Postmortem Interval
WB: Western Blotting

Figure Legends

Figure 1 – Gene ontology (GO) analysis and characterization of SERBP1-interacting proteins. A) SERBP1-interacting factors were identified via pull-down analysis in 293T cells. GO enrichment analysis (Biological Processes, Molecular Function, and Cellular Component) was performed with ShinyGO (27). A selection of the most relevant GO terms is represented. FE = fold enrichment; FDR = false discovery rate. **B)** Visualization of associated GO-enriched terms in three main regulatory branches: translation, ribosome biogenesis, and RNA processing. Sum and circle size represent the count of SERBP1 interactors assigned to each GO term. **C)** Representation of top enriched protein domains according to PFAM (42) among SERBP1 interactors. Only PFAM domains with counts of 5 or more and significant fold enrichment (FE) and false discovery rate (FDR) were included. The occurrence of each domain within the total human proteome (ALL) is listed as a reference. **D)** Occurrence of intrinsically disordered proteins (IDPs) (45) among SERBP1 interactors according to PFAM ("derived" = automatic entries from databases; "curated" = manually checked). **E)** Distribution of identified SERBP1-interacting proteins in reference to the presence of RGG boxes (50) and binding to G-quadruplexes (G4s) (46, 47). Data used to generate the figures are in Tables S1, S4 and S6.

Figure 2 – SERBP1 is implicated in cell division. A) SERBP1-associated proteins and their presence in specific cellular structures relevant to mitosis. **B)** Western blot showing SERBP1 knockdown in U251 and U343 cells. **C)** Multinucleated cells in U251 and U343 control and SERBP1 knockdown (KD) cells after treatment with paclitaxel, an agent that causes cell cycle arrest. SERBP1 KD increased the number of multinucleated nuclei. Data are shown as means of counts of 1000 cells ± standard deviation (in triplicate) and statistical significance was determined by Student's t-test. $P<0.001$. **D)** Aspect of cells exposed to paclitaxel. On the left staining with anti-α-Tubulin; in the middle staining with DAPI showing an increased number of multinucleated cells after siSERBP1 KD. 100X magnification for detailed visualization of a single multinucleated cell. **E)** Plot shows the results of a cell viability screening (291 drugs) performed in U343 control vs. U343 SERBP1 over-expressing (OE) cells. Red dots correspond to drugs whose impact on cell viability was significantly different between U343 control and U343 SERBP1 OE. **F)** Highlights of the screening showing cell cycle/division and DNA damage/replication inhibitors whose impact on cell viability was smaller in U343 SERBP1 OE in comparison to control. Datasets used to prepare the figure and detailed analysis are in Table S1 and S7.

Figure 3 – SERBP1 influences splicing. A) SERBP1-interacting factors are preferentially associated with splicing. Networks show connections between splicing factors identified as SERBP1 interactors. **B)** SERBP1 knockdown in U251 cells produced major changes in splicing. Pie chart displays the distribution of splicing events affected by SERBP1 knockdown according to their type: SE, exon skipping; RI, intron retention; MXE, multiple exclusive exons; A5SS, alternative 5' splice sites; A3SS, alternative 3' splice site. **C)** Bar graphs showing the percentage of splicing events affected by SERBP1 knockdown with evidence of SERBP1 binding sites close (<100nt) to regulated splice sites. **D)** hnRNPU was identified as a potential partner of SERBP1 in splicing regulation. SERBP1 and hnRNPU display high expression correlation in normal and tumor tissues. **E)** Venn diagram shows a strong overlap between the splicing events affected by SERBP1 and hnRNPU knockdowns in U251 cells. **F)** Sashimi plots showing examples of splicing events affected by both SERBP1 and hnRNPU knockdowns in U251 cells. The red arrows indicate affected exons. Datasets used to prepare the figure and detailed analyses are in Table S8.

Figure 4 – SERBP1 interacts with PARP1 and influences PARylation. A) Results of IP-western in U251 cells with control and anti-SERBP1 antibodies confirm SERBP1 interaction with PARP1, NCL and SYNCRIP. SERBP1 and PARP1 strong association is corroborated by their high expression correlation in different studies **(B)** and similar expression profiles during cortex development according to Cortecon (142). **(C) . D)** PARylation sites observed in SERBP1 protein according to (62, 63). **E)** PARP1 ADP-ribosylates SERBP1 *in vitro*. Purified recombinant PARP1 (0.1 µM) and SERBP1 (0.6 µM) were combined in a reaction with or without sheared salmon sperm DNA (sssDNA) (100 ng/µL) and NAD+ (100 µM) as indicated. The reaction products were analyzed by SDS-PAGE with silver staining (left) and Western blotting for PAR (right). Uncropped gels are shown. **F)** Venn diagram shows that majority of SERBP1-associated factors get PARylated and/or bind PAR (62–64). **G)** Increase of PARylation levels in 293T and U251 GBM cells after H_2O_2 treatment. **H)** SBP-SERBP1 and Flag-PARP1 were co-transfected into 293T cells. Cells were treated with H_2O_2 to induce PARylation and a pull-down experiment with streptavidin beads was performed. Western analysis showed increased SERBP1 association with PARP1 in cells treated with H_2O_2. SBP-SERBP1-His detected by His antibody; Flag-PARP1 detected by Flag antibody. **I)** SBP-SERBP1 was transfected into 293T cells. Cells were treated with DMSO or 10µM PJ34 (PARP inhibitor) for two hours and a pull-down experiment with streptavidin beads was performed. Western analysis showed a decrease in SERBP1 association with PARP1 and GPBP1. **J)** SERBP1 transgenic expression (mGreen-SERBP1) in 293T cells increased the levels of PARylated proteins as indicated by PAR-detecting agent. Datasets used to prepare the figure and detailed analyses are in Tables S1, S5 and S6.

Figure 5 – Shared SERBP1 and PARP1 interactors. A) Venn diagram shows the overlap between PARP1 (66) and SERBP1 interactomes. Analysis of shared interactors indicated that the majority of them are PAR binding (64) and/or get PARylated (62, 63). **B)** Selection of enriched GO terms (biological processes) related to SERBP1-PARP1 shared interactors according to ShinyGO (27). FE = fold enrichment; FDR = false discovery rate. **C)** Network showing shared SERBP1 and PARP1 interactors implicated in ribosome biogenesis. **D)** Proposed SERBP1-PARP1 feedback model; SERBP1 function and association with partner proteins is modulated by PARylation while SERBP1 influences PARP activity. Datasets used to prepare the figure and detailed analyses are in Tables S1 and S6.

Figure 6 – SERBP1-associated proteins are present in membraneless organelles. A) Different types of membraneless organelles in a cell and examples of SERBP1-associated proteins present in each structure. **B)** Membraneless organelles identified in the GO enrichment analysis (cellular component) of SERBP1 interactors (72). FE = fold enrichment; FDR = false discovery rate. **C)** Bar graph showing the distribution of SERBP1-associated proteins in different membraneless organelles. **D)** Venn diagram representing the distribution of SERBP1-associated proteins present in membraneless organelles in respect to G4 binding (46, 47), PAR binding (64), and PARylation (62, 63). Datasets used to prepare the figure and detailed analyses are in Tables S1, S6 and S9.

Figure 7 – SERBP1 is present in Tau aggregates. A) Representative co-immunofluorescence of SERBP1 and Phospho-Tau (Thr231) in AD brain tissues. Merged channel is represented. DAPI was used to stain nuclei. Magnification 20x and white scale bar: 50 µm. Three different Insets selected from merged channels are represented in zoomed images as merged, SERBP1 (green) and Phospho-Tau (red). **B)** Representative PLA of SERBP1 vs. pTau in AD and aged-matched control brains (magnification 40x and white scale bar: 50µm). **C)** Percentage of positive area to PLA fluorescence in region of interests in AD and control brains (Ctr vs AD, *** *$p<0.001$*, paired t-test). **D)** Western blot showing SERBP1 expression in normal and AD brains

and presence of oligomers. GAPDH and Tau oligomers immunoblot are shown. **E)** SERBP1 relative density in Ctr and AD brains, quantified as function of GAPDH (from immunoblot in D). (Ctr vs. AD, * *p<0.05*, paired t-test). **F)** Venn diagram shows overlap between proteins often identified in Tau aggregates and SERBP1 associated proteins identified in this study (top). Gene Ontology (GO) enrichment analysis (Biological Processes) using ShinyGO (27) indicated that SERBP1-associated factors that are also present in Tau aggregates are implicated in ribosome biogenesis, translation, splicing and telome maintenance. FE = fold enrichment; FDR = false discovery rate. Datasets used to prepare the figure and detailed analyses are in Tables S1 and S9.

Figure 8 – SERBP1 association with PARP1 in Alzheimer's brains. A) Representative co-immunofluorescence of SERBP1 and PARP1 in AD and age-matched control brain tissues. PARP1 and SERBP1 are represented in gray while merged images represent PARP1 (red), SERBP1 (green). DAPI was used to stain nuclei (blue). Magnification 20x and white scale bar: 100 µm. Each frame has a zoomed inset representing the detailed distribution of each target. **B)** Pearson Coefficient (PCC) of co-localizing SERBP1 and PARP1 between cells of age-matched control and AD brains (CTR vs. AD, **** p<0.001 paired t-test). **C**) Fluorescence intensity profiles of PARP1 (red), SERBP1 (green), and DAPI (blue) in representative cells from age-matched control and AD brains. Distance is represented in pixels and fluorescence intensity as Grey value obtained using ImageJ FIJI software. **D)** Representative PLA of SERBP1 vs. PARP1 in AD and aged-matched control brains (magnification 40x and white scale bar: 50µm). Percentage of positive area to PLA fluorescence in region of interests in AD and control brains (Ctr vs AD, ** *p<0.01*, paired t-test).

A

Biological Process

Pathway	FE	FDR
SRP-dependent cotranslational protein targeting to membrane		
Translational initiation		
Ribosome biogenesis		
Translation		
Translational elongation		
RNA splicing		
mRNA processing		
RNA processing		
RNA 3-end processing		
Ribonucleoprotein complex biogenesis		
Ribonucleoprotein complex localization		
RNA localization		
RNA transport		
mRNA transport		
Nucleocytoplasmic transport		
Regulation of establishment of protein localization to telomere		
Regulation of telomere maintenance		
Regulation of chromosome organization		
DNA repair		

FE: 2.8 – 31.5

FDR: 3.2×10^{-8} – 4.4×10^{-166}

Molecular Function

Pathway	FE	FDR
DNA/RNA helicase activity		
Catalytic activity, acting on RNA		
Structural constituent of ribosome		
Translation initiation factor activity		
Translation factor activity, RNA binding		
Translation regulator activity		
N6-methyladenosine-containing RNA binding		
Sequence-specific mRNA binding		
snoRNA binding		
rRNA binding		
miRNA binding		
snRNA binding		
tRNA binding		
Ribonucleoprotein complex binding		
Cadherin binding		
Cell adhesion molecule binding		
Telomeric DNA binding		
Chromatin binding		

FE: 3.2 – 32.5

FDR: 5.2×10^{-4} – 2.3×10^{-72}

Cellular Component

Pathway	FE	FDR
Translation preinitiation complex		
Polysome		
Ribosome		
CRD-mediated mRNA stability complex		
U2-type prespliceosome		
Spliceosomal complex		
Methyltransferase complex		
Cytoplasmic stress granule		
Ribonucleoprotein complex		
Sno(s)RNA-containing ribonucleoprotein complex		
Cajal body		
Nuclear speck		
Chromosomal region		
Focal adhesion		
Anchoring junction		
Postsynaptic specialization		
Postsynaptic density		

FE: 3.0 – 43.3

FDR: 2.3×10^{-4} – 1.1×10^{-201}

B

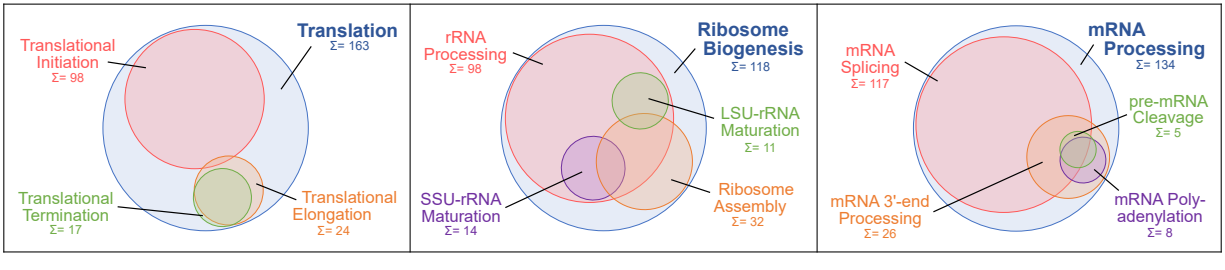

C

PFAM	Domain	SER	ALL	FE	FDR
PF00076	RNA recognition motif (a.k.a. RRM, RBD, or RNP domain)	63	754		
PF00271	Helicase conserved C-terminal domain	32	285		
PF00270	DEAD/DEAH box helicase	28	222		
PF00400	WD domain, G-beta repeat	23	669		
PF00013	KH domain	10	124		
PF07717	Oligonucleotide/oligosaccharide-binding (OB)-fold	9	33		
PF04408	Helicase associated domain (HA2)	9	35		
PF00118	TCP-1/cpn60 chaperonin family	8	52		
PF01399	PCI domain	7	51		
PF00012	Hsp70 protein	7	61		
PF00538	linker histone H1 and H5 family	6	21		
PF00244	14-3-3 protein	6	26		
PF00009	Elongation factor Tu GTP binding domain	6	53		
PF02037	SAP domain	6	54		
PF03144	Elongation factor Tu domain 2	5	27		

RNA binding motif

RNA binding + helicase motif

FE: 2.5 – 21.1

FDR: 2.7×10^{-3} – 2.5×10^{-27}

D

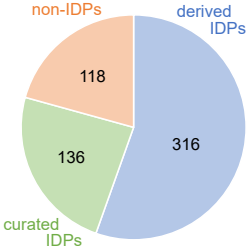

E

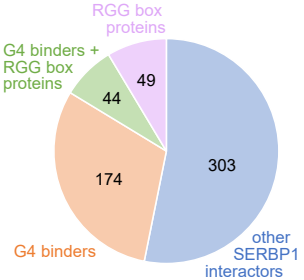

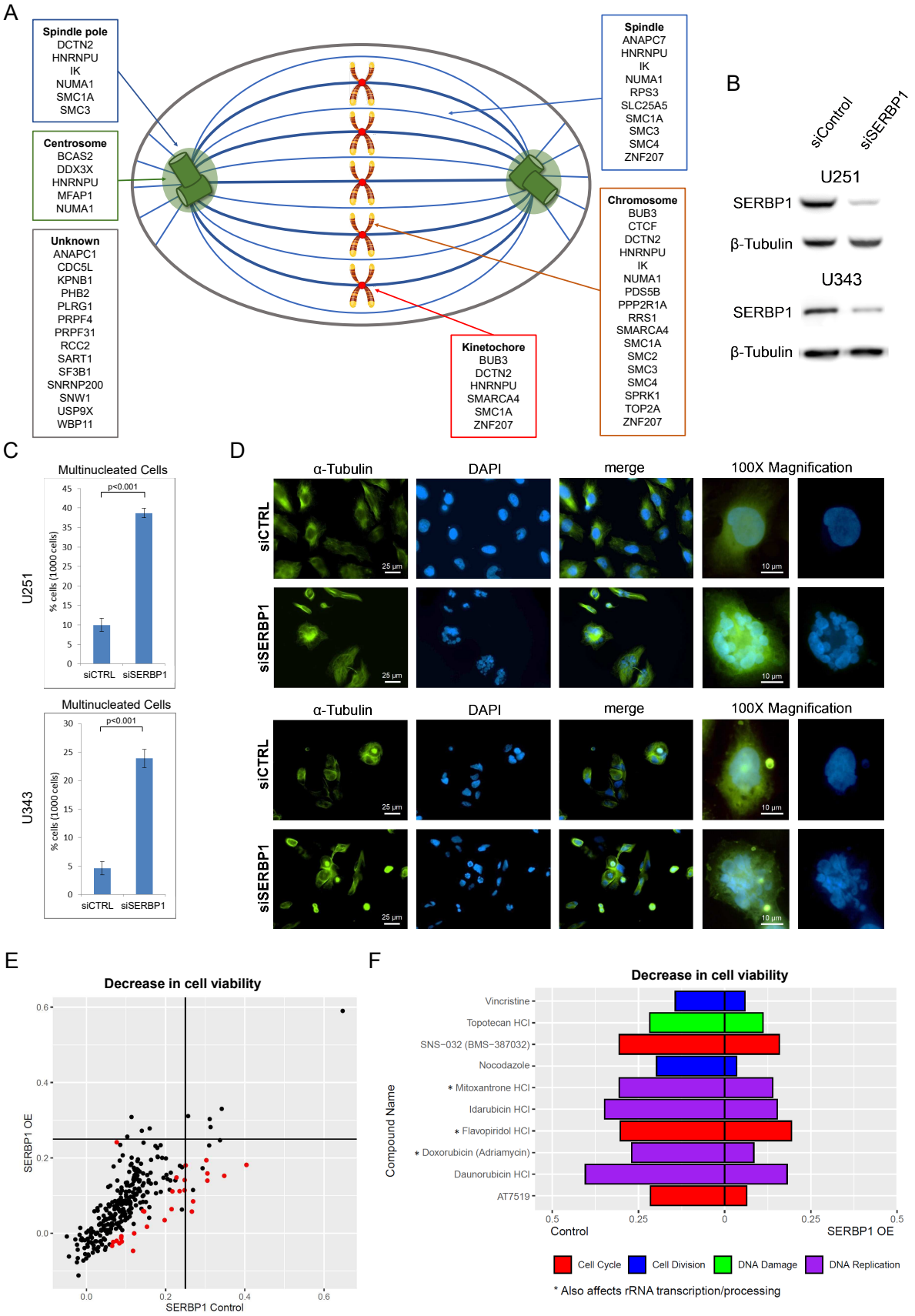
A
Spindle pole
DCTN2
HNRNPU
IK
NUMA1
SMC1A
SMC3
Centrosome
BCAS2
DDX3X
HNRNPU
MFAP1
NUMA1
Unknown
ANAPC1
CDC5L
KPNB1
PHB2
PLRG1
PRPF4
PRPF31
RCC2
SART1
SF3B1
SNRNP200
SNW1
USP9X
WBP11
Spindle
ANAPC7
HNRNPU
IK
NUMA1
RPS3
SLC25A5
SMC1A
SMC3
SMC4
ZNF207
Chromosome
BUB3
CTCF
DCTN2
HNRNPU
IK
NUMA1
PDS5B
PPP2R1A
RRS1
SMARCA4
SMC1A
SMC2
SMC3
SMC4
SPRK1
TOP2A
ZNF207
Kinetochore
BUB3
DCTN2
HNRNPU
SMARCA4
SMC1A
ZNF207
B
siControl
siSERBP1
U251
SERBP1
β-Tubulin
U343
SERBP1
β-Tubulin
C
Multinucleated Cells
p<0.001
% cells (1000 cells)
U251
siCTRL
siSERBP1
Multinucleated Cells
p<0.001
% cells (1000 cells)
U343
siCTRL
siSERBP1
D
α-Tubulin
DAPI
merge
100X Magnification
siCTRL
siSERBP1
25 µm
10 µm
α-Tubulin
DAPI
merge
100X Magnification
siCTRL
siSERBP1
25 µm
10 µm
E
Decrease in cell viability
SERBP1 OE
SERBP1 Control
F
Decrease in cell viability
Compound Name
Vincristine
Topotecan HCl
SNS-032 (BMS-387032)
Nocodazole
* Mitoxantrone HCl
Idarubicin HCl
* Flavopiridol HCl
* Doxorubicin (Adriamycin)
Daunorubicin HCl
AT7519
Control
SERBP1 OE
Cell Cycle
Cell Division
DNA Damage
DNA Replication
* Also affects rRNA transcription/processing

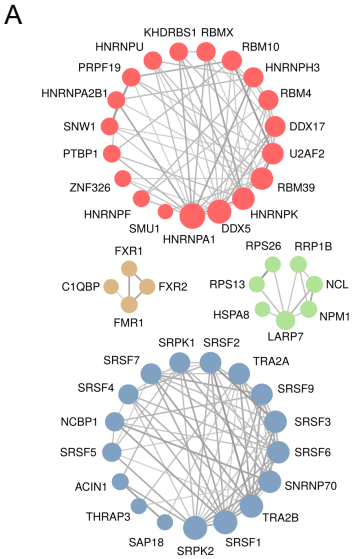

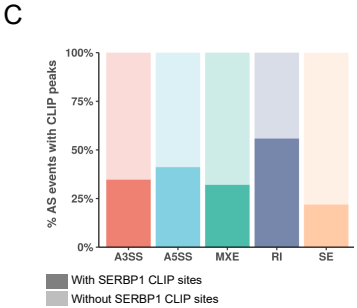

D

SERBP1 vs. hnRNPU expression correlation

	r-value	r-pvalue
Brain Hardy	0.699	1.04×10^{-178}
TCGA GBM	0.320	1.01×10^{-03}
Ivy GAP GBM	0.578	
Neuroblastoma	0.592	1.22×10^{-45}
Pancreatic Adenocarcinoma	0.302	2.83×10^{-04}
Bladder Urothelial Carcinoma	0.542	8.72×10^{-30}
Sarcoma	0.330	2.43×10^{-06}

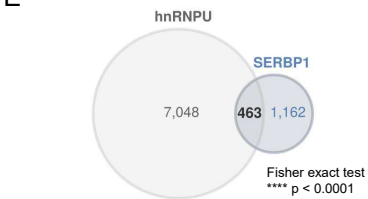

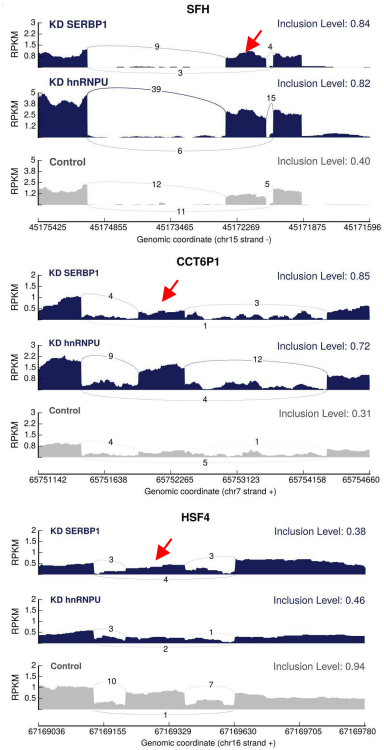

A

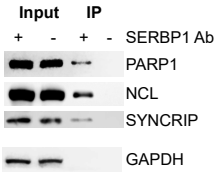

B

SERBP1 vs. PARP1 expression correlation

	r-value	r-pvalue
Brain Hardy	0.596	8.70×10^{-118}
TCGA GBM	0.325	8.12×10^{-04}
Neuroblastoma	0.549	2.38×10^{-38}
Bladder Urothelial Carcinoma	0.371	1.65×10^{-13}
Sarcoma	0.326	3.24×10^{-06}

C

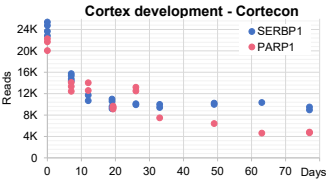

D

SERBP1 PARylation Sites

AA Site	Site ± 8 AA
200	EFDRHSGSD*RSSFSHYS
233	GTVKDELTE*SPKYIQKQ
329	KGFVLHKSK*SEEAHAED
398	DKSSASAPD*VDDPEAFP
401	SASAPDVDD*PEAFPALA
403	SAPDVDDPE*AFPALA

E

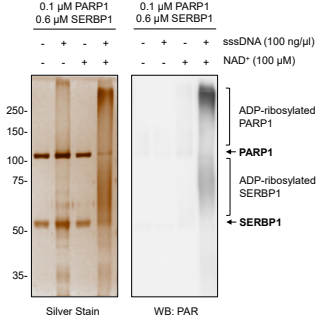

F

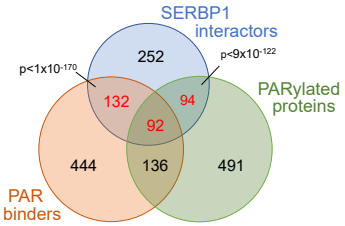

G

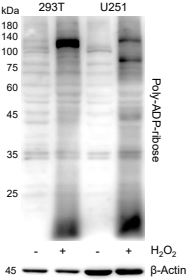

H

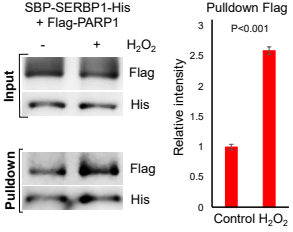

I

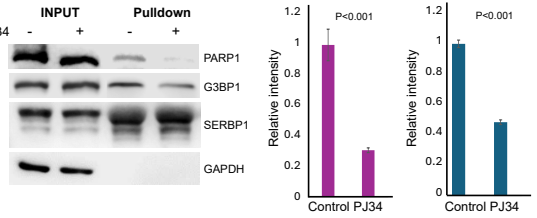

J

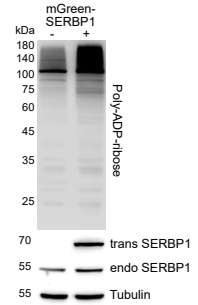

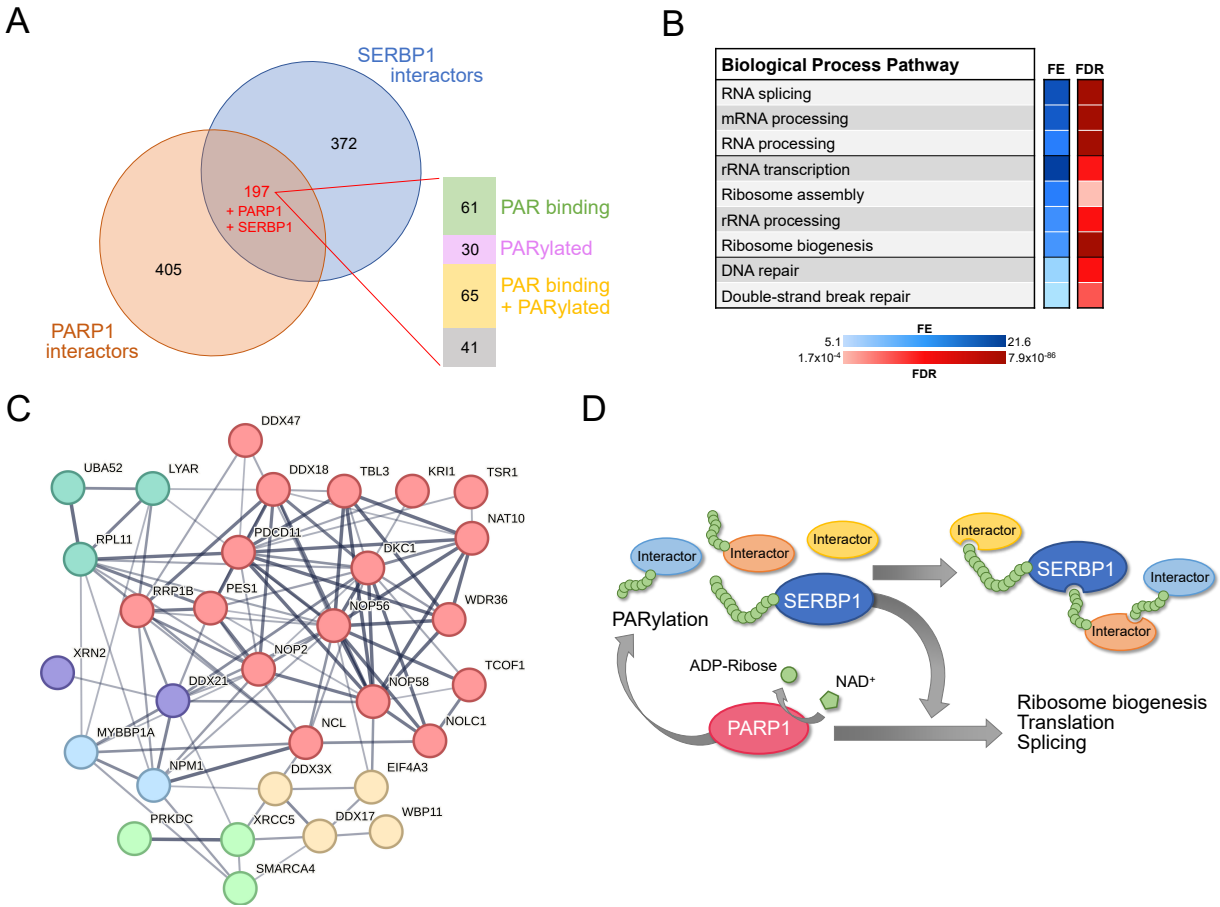
A
SERBP1 interactors
372
197
+ PARP1
+ SERBP1
405
PARP1 interactors
61
PAR binding
30
PARylated
65
PAR binding + PARylated
41
B
Biological Process Pathway
FE
FDR
RNA splicing
mRNA processing
RNA processing
rRNA transcription
Ribosome assembly
rRNA processing
Ribosome biogenesis
DNA repair
Double-strand break repair
FE
5.1
21.6
FDR
1.7x10-4
7.9x10-86
C
DDX47
UBA52
LYAR
DDX18
TBL3
KRI1
TSR1
NAT10
RPL11
PDCD11
DKC1
RRP1B
PES1
NOP56
WDR36
XRN2
NOP2
TCOF1
DDX21
NOP58
NCL
NOLC1
MYBBP1A
NPM1
DDX3X
EIF4A3
PRKDC
XRCC5
DDX17
WBP11
SMARCA4
D
Interactor
Interactor
Interactor
Interactor
SERBP1
SERBP1
Interactor
Interactor
PARylation
ADP-Ribose
NAD+
PARP1
Ribosome biogenesis
Translation
Splicing

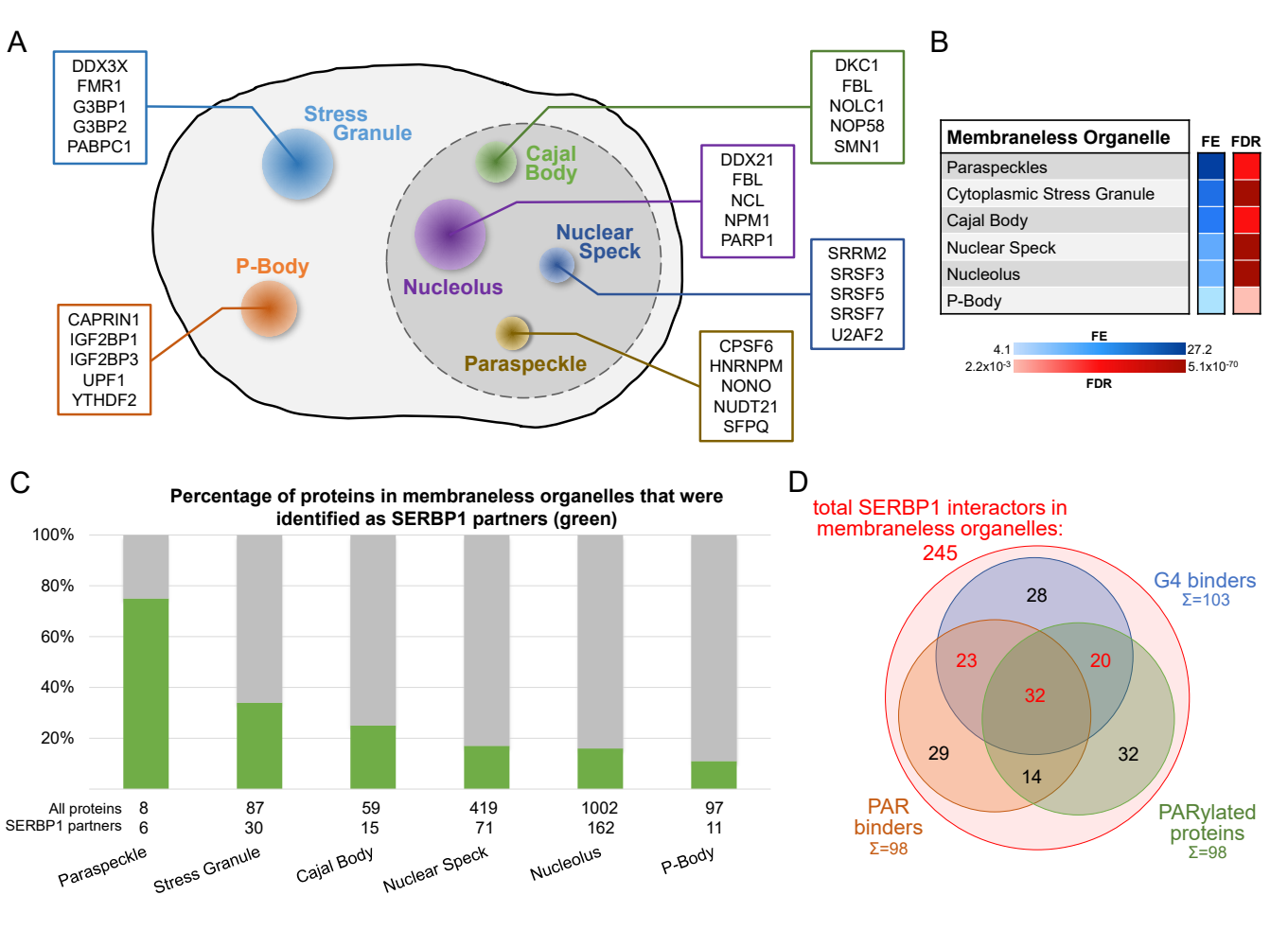
A
DDX3X
FMR1
G3BP1
G3BP2
PABPC1
Stress Granule
Cajal Body
DKC1
FBL
NOLC1
NOP58
SMN1
DDX21
FBL
NCL
NPM1
PARP1
Nuclear Speck
SRRM2
SRSF3
SRSF5
SRSF7
U2AF2
P-Body
Nucleolus
CAPRIN1
IGF2BP1
IGF2BP3
UPF1
YTHDF2
Paraspeckle
CPSF6
HNRNPM
NONO
NUDT21
SFPQ
B
Membraneless Organelle
FE
FDR
Paraspeckles
Cytoplasmic Stress Granule
Cajal Body
Nuclear Speck
Nucleolus
P-Body
FE
4.1
27.2
2.2x10-3
5.1x10-70
FDR
C
Percentage of proteins in membraneless organelles that were identified as SERBP1 partners (green)
100%
80%
60%
40%
20%
All proteins 8 87 59 419 1002 97
SERBP1 partners 6 30 15 71 162 11
Paraspeckle
Stress Granule
Cajal Body
Nuclear Speck
Nucleolus
P-Body
D
total SERBP1 interactors in membraneless organelles:
245
G4 binders
Σ=103
28
23
20
32
29
32
14
PAR binders
Σ=98
PARylated proteins
Σ=98

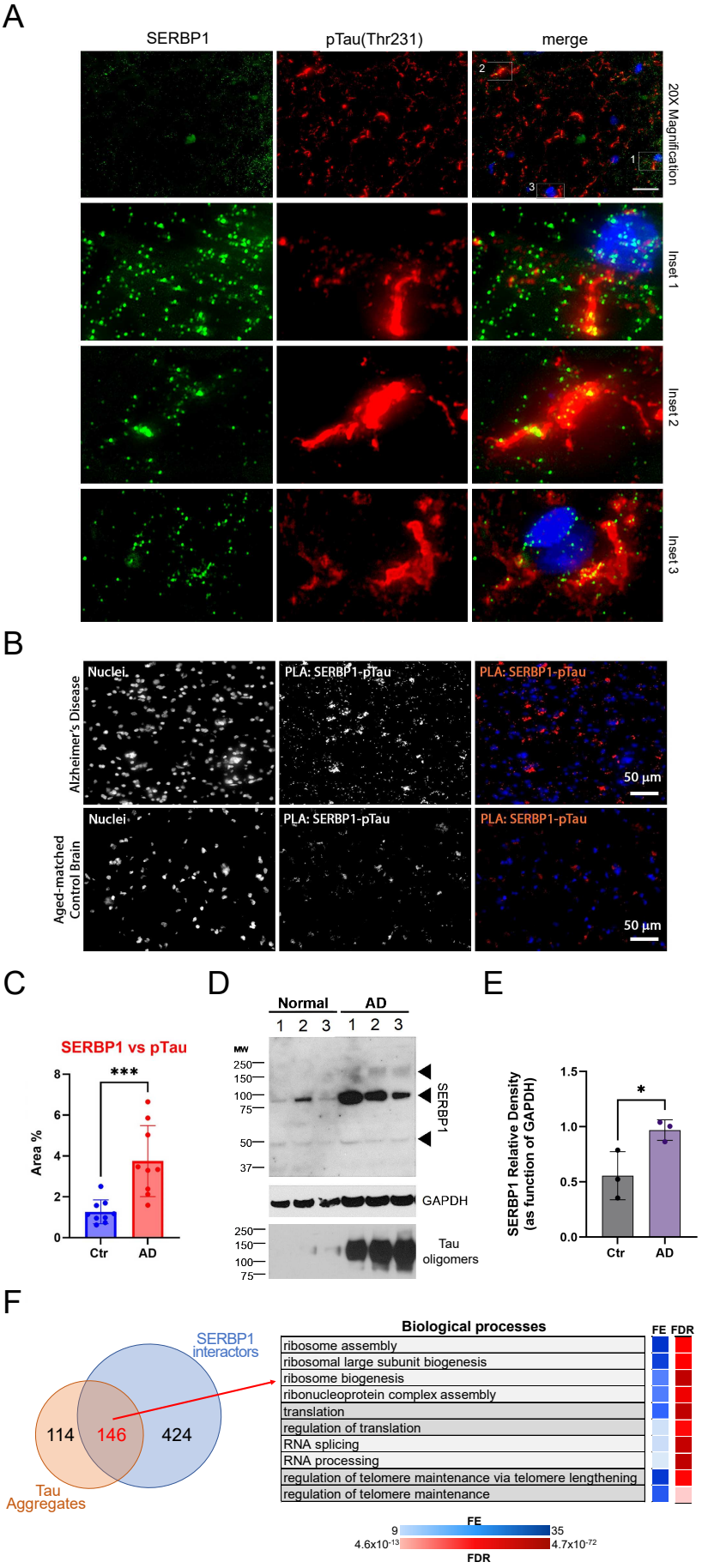
A
SERBP1
pTau(Thr231)
merge
20X Magnification
Inset 1
Inset 2
Inset 3
B
Alzheimer's Disease
Aged-matched Control Brain
Nuclei
PLA: SERBP1-pTau
50 µm
C
SERBP1 vs pTau
***
Area %
Ctr
AD
D
Normal
AD
MW
SERBP1
GAPDH
Tau oligomers
E
SERBP1 Relative Density (as function of GAPDH)
*
Ctr
AD
F
SERBP1 interactors
Tau Aggregates
114
146
424
Biological processes
FE
FDR
ribosome assembly
ribosomal large subunit biogenesis
ribosome biogenesis
ribonucleoprotein complex assembly
translation
regulation of translation
RNA splicing
RNA processing
regulation of telomere maintenance via telomere lengthening
regulation of telomere maintenance
FE
9
35
FDR
4.6x10-13
4.7x10-72

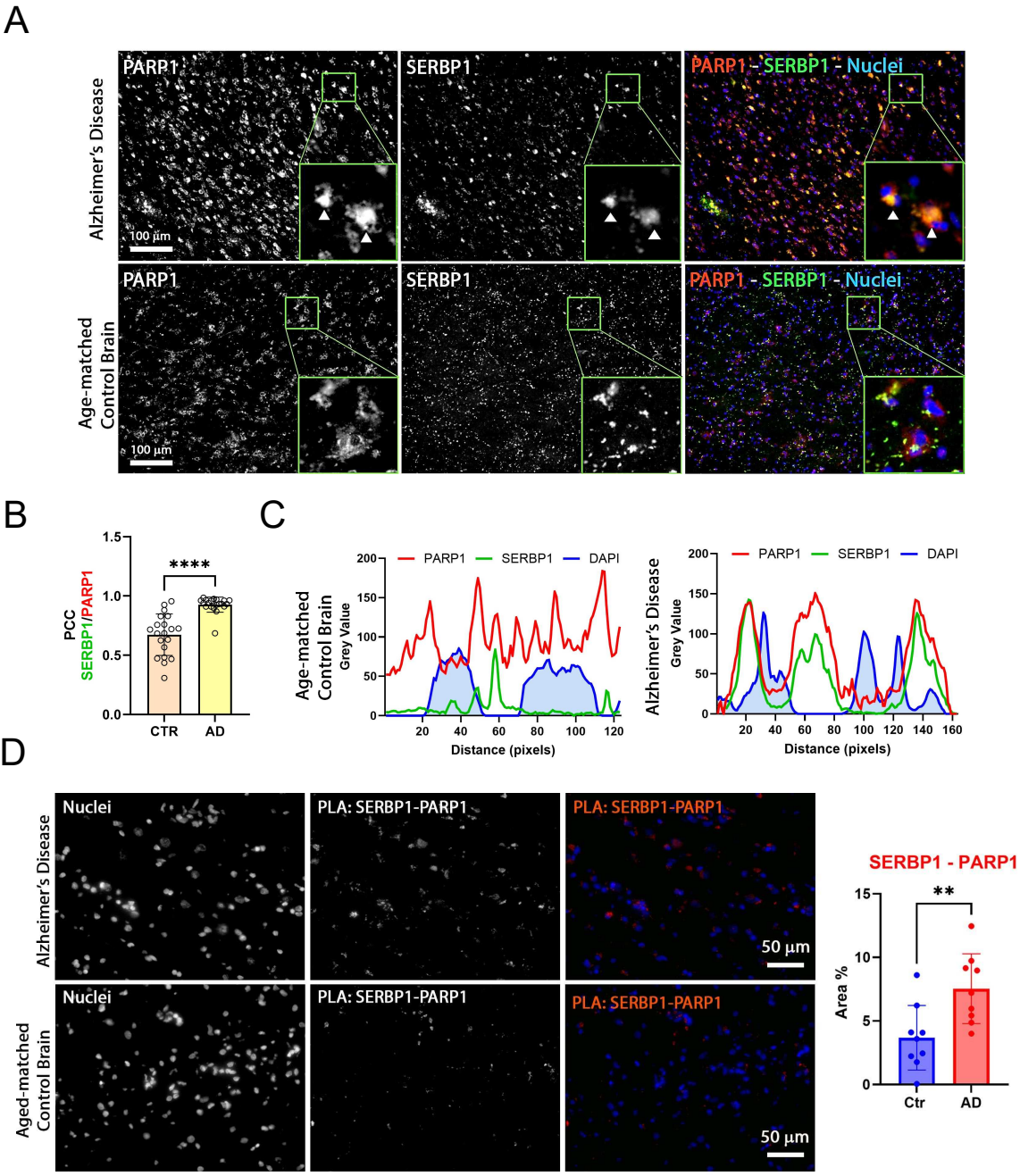
A
Alzheimer's Disease
Age-matched Control Brain
PARP1
SERBP1
PARP1 - SERBP1 - Nuclei
100 µm
B
PCC SERBP1/PARP1
****
CTR
AD
C
Age-matched Control Brain
Alzheimer's Disease
Grey Value
Distance (pixels)
PARP1
SERBP1
DAPI
D
Nuclei
PLA: SERBP1-PARP1
Aged-matched Control Brain
50 µm
SERBP1 - PARP1
Area %
**
Ctr
AD